

Case study



Sustainable utilization of red mud waste (bauxite residue) and slag for the production of geopolymers composites: A review

Shaker M.A. Qaidi^a, Bassam A. Tayeh^{b,*}, Haytham F. Isleem^c, Afonso R. G. de Azevedo^d, Hemn Unis Ahmed^e, Wael Emad^f

^a Department of Civil Engineering, College of Engineering, University of Duhok, Duhok, Kurdistan Region, Iraq

^b Civil Engineering Department, Faculty of Engineering, Islamic University of Gaza, P.O. Box 108, Gaza Strip, Palestine

^c Department of Construction Management, Qujing Normal University, Qujing 655011, Yunnan, China

^d UENF - State University of the Northern Rio de Janeiro, LECIV – Civil Engineering Laboratory, Av. Alberto Lamego, 2000, 28013-602 Campos dos Goytacazes, RJ, Brazil

^e Civil Engineering Department, College of Engineering, University of Sulaimani, Sulaimaniyah, Kurdistan Region, Iraq

^f Department of Civil Engineering, Komar University of Science and Technology, Kurdistan-Region, Iraq

ARTICLE INFO

Keywords:

Red mud
Slag
Geopolymers, mechanical, durability, and microstructure properties
Life cycle assessment
Radioactive
Economic and environmental impacts

ABSTRACT

The production of cement results in the emission of much carbon dioxide, which contributes to undesirable environmental impacts such as climate change and global warming. These phenomena have rekindled interest in utilizing a variety of industrial waste products to produce geopolymers (GP) composites and alkali-activated (AA) binders in order to reduce the usage of ordinary Portland cement in building construction. Waste red mud (RM), also known as bauxite residue, is one of these hazardous radioactive waste materials that is formed as a by-product of Bayer's aluminum manufacturing process. This paper conducts a systematic review of the literature on the use of RM and slag in the production of red mud-slag geopolymers (RM-SGP). An overview of the economic and environmental impacts, physical and chemical properties, production, distribution, classification, and potential applications of RM are presented. Besides, recent advancements in the usage of RM and slag for geopolymers production are described in terms of physical, mechanical, durability, and microstructure properties. Moreover, this study attempts to chart a route toward a realistic valorization that reflects both real and perceived concerns, such as radioactivity, leaching, and the life cycle assessment of red mud geopolymers (RM-GP). The potential use of RM-SGP production indicates the need for further studies into the mixture proportion and combination of these two raw ingredients with other cementitious materials leading to new energy-saving and affordable building products and processes. Also, it is recommended that research efforts be directed toward economic, life cycle, and environmental assessments.

1. Introduction

Waste reduction in industrial and mining sectors has been an environmental and climate change priority in latest years [1–3]. It is vital, thus, to create technological innovations for the conversion of wastes into value-added products [4–7]. AA binders/GPs are a type

* Corresponding author.

E-mail address: btayeh@iugaza.edu.ps (B.A. Tayeh).

of cementitious binder that may be synthesized from industrial wastes with an alumino-silicate component and pushed as a substitute for conventional cement [8–11]. These alumino-silicate minerals may originate from geological sources or industrial by-products containing alumino-silicates, like RM. These materials can be used alone or in conjunction with other materials. ↗.

Recycling these industry items can help to reduce the complexity that may have a negative impact on the environment and people's health [12–15]. Furthermore, by substituting GP binders for cement, energy connected with cement manufacture may be saved, as well as CO₂ emissions created by carbonate incineration [16–18].

RM waste (bauxite residue) formed by the aluminum industry as a result of the Bayer process for extracting alumina (Al₂O₃) from bauxite ore, which involves treating bauxite ore with a solution of sodium hydroxide [19–21]. The production of RM is estimated to be between 1.5 and 2.5 tonnes per tonne of Al₂O₃, depending on the source and effectiveness of the extraction procedure [22,23]. The majority of these pollutants are either dumped on lands or discharged into the ocean after they have been neutralized [24–26]. Owing to its large alkalinity and cation exchange capability, RM storage consumes a large amount of area and poses a major hazard to the soil, environment, and water [27]. The leaching of toxic substances from RM can damage soil and poison groundwater. Therefore, safe disposal and complete exploitation of RM become critical concerns for the Al₂O₃ sector, given the industry's massive resource consumption and substantial environmental difficulties. ↗.

Although the material's extremely alkaline nature precludes reuse, it finds successful application in GP technologies due to the inclusion of SiO₂ and Al₂O₃ in addition to Na₂O [28–31]. Recycling and reuse are viable options for treating RM in order to minimize adverse impacts on the environment while being economically viable [32]. ↗.

The dangers associated with RM dumping encourage the efficient use of RM in building materials/civil application areas. It is used in the manufacture of clinker [17,33,34], hollow/foamed bricks [14,24,35], paving blocks [36], RM as clay ↗ substitute for fired brick production [37,38], red ↗ mud bricks [39], ↗ partial substitution of ↗ cement [40,41], specific cement [42], lightweight aggregate [43–46], specific cement [42], as a binder or additive in concrete and mortars [47,48], ceramic ↗ tiles [49–51], and as packings in polymer composites [52–56]. ↗.

2. Production of bauxite, alumina (Al₂O₃), and RM

Bauxite is one of the most significant naturally occurring sources for making aluminum, ↗ accounting for approximately 97% of the aluminum produced globally [57]. Bauxite is a natural ore that is composed mostly of aluminum hydroxide minerals like diaspore ↗(a-Al(OH)₄), boehmite (c-Al(OH)₄), and gibbsite (aluminum hydroxide) [58]. Additionally, bauxite ↗ includes impurities like hematite (a-Fe₂O₃), quartz (SiO₂), kaolinite (Al₂Si₂O₅(OH)₄), and ↗ anatase/rutile (TiO₂) [58].

Due to the mineral content of bauxite deposits varying, many aluminum manufacturing processes ↗ have been developed, comprising the Bayer process, the sintering process, and a combination ↗ Bayer-sintering process. In Fig. 1, the proposed process's streamlined flow diagram is compared ↗ to those of the Bayer and sinter processes. The Bayer process consists of digestion and leaching

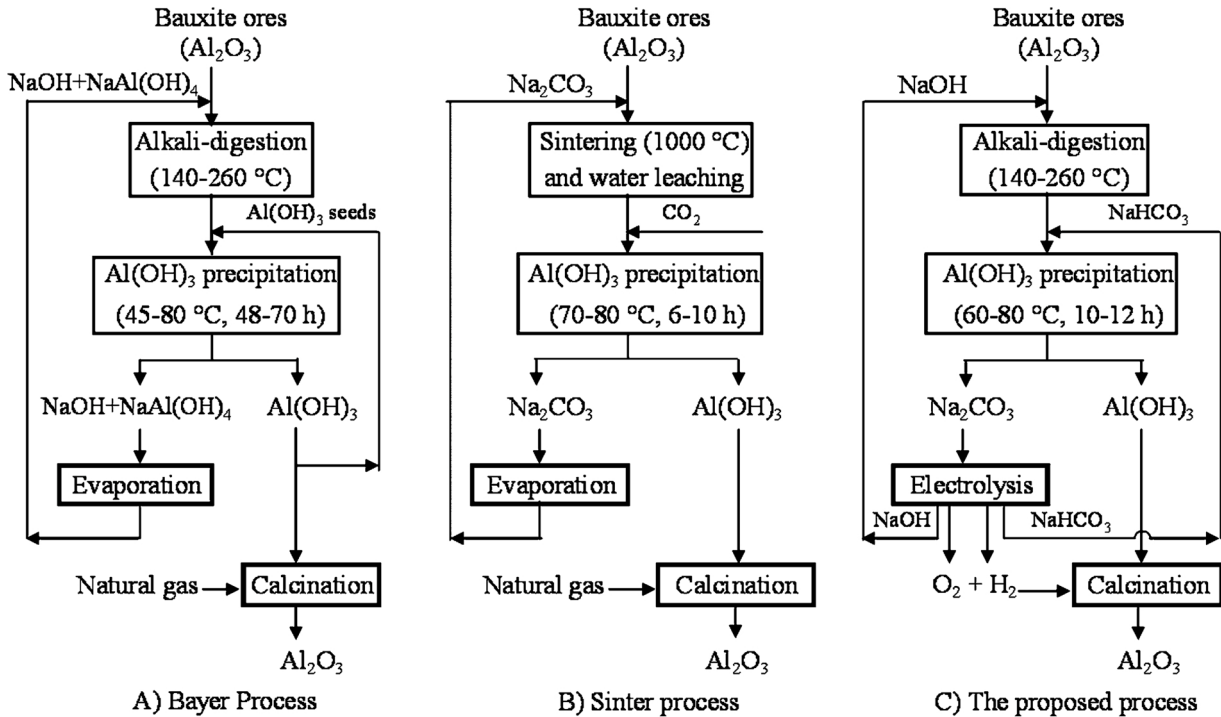


Fig. 1. Simplified flow diagrams of aluminum manufacturing processes ↗[63].

the ores with a hot alkali solution and precipitating aluminum hydroxide from super-saturated aluminate leachate utilizing aluminum hydroxide seeding particles [59]. The residual caustic liquor is reduced by evaporation and returned to the mining process, as illustrated in Fig. 1-A. The sintering process entails sintering the ores with calcium oxide and sodium carbonate at temperatures greater than 1000 °C, leaching the sinter volume with crystallizing aluminum hydroxide and water (or dilute sodium hydroxide solution) using CO₂, capitalizing the spent green liquor via evaporation, and making the rounds the concentrate to the next sinter stage, as illustrated in Fig. 1-B. The combined Bayer-sintering process (proposed processes) is a created methodology based on the regular Bayer process with the objective of alleviating the problem of excessive SiO₂ concentration in certain bauxite ores. As illustrated in Fig. 1-C, this process began with a typical Bayer caustic leaching of the high-SiO₂ bauxite. The RM-containing sodium aluminum silicates were then sintering, accompanied by a water leaching procedure to recover soda and Al₂O₃ [60,61]. While the sintering process is more efficient than the Bayer process for low-grade diaspore ores, its high energy consumption renders it costly in comparison to the Bayer process, and its ecological cost has been a major concern.

With technological innovations, the need for bauxite production has expanded dramatically in relation to world Al utilization, resulting in a vast creation of bauxite residue, commonly known as RM. Table 1 summarizes worldwide bauxite output from 1970 to 2019.

Power, Gräfe and Klauber [62] predicted yearly RM production at 120 M.t and a global stockpile of more than 2.65 B.t in 2007. Depending on yearly Al₂O₃ production statistics depicted in Figs. 2 and 3 from 1998 to 2015, it may be deduced that RM output increased overall. Knowing that 2–3 tonnes of bauxite are required to generate 1 tonne of Al₂O₃ in the Bayer process, the quantity of RM generated may be calculated by applying an average ratio of 1.5 to Al₂O₃ production statistics [62], which results in roughly 170 M.t of RM produced globally in 2015. The volume of RM generated annually in various countries is shown in Fig. 4.

3. Distribution and classification and of bauxite ores

Bauxite is an aluminum ore that is well identified as a key source of aluminum [70,71]. It is often composed of a variety of minerals, including (aluminum hydroxide), diaspore (α -AlO(OH)), and boehmite (γ -AlO(OH)) blended with the goethite, kaolinite, hematite, and slight quantities of ilmenite (FeTiO₃ or FeO.TiO₂) and anatase (TiO₂) [72]. These bauxite ores have highly distinct crystal forms. According to its structure, bauxite ore is classed as gibbsitic, diasporic, or boehmitic [65,73]. Table 2 and Fig. 5 illustrate the various forms of bauxite found in various countries.

4. Environmental impacts of RM

Owing to the increased alkali content of RM, it is classified as toxic waste, constituting threats to the environment in the situation of improper disposal [73,78]. RM is often dumped at RM ponds, bauxite residue dumpsites [79–82], and abandoned bauxite mines as dried or semi-dry materials [83,84]. The majority of RM is stored in open-air dams, which not only consume enormous amounts of fertile land but also lead to air and environmental pollution through alkali leakages into groundwater, storage instabilities, and fugitive dust emissions [85,86].

The high amount of free Na⁺ in RM precludes the formation of coordination bonds with negatively charged surfaces or the formation of additional stable hydration layers. It results in the production of a white surface of precipitating chloride on the residue's surfaces [87], as well as the disintegration of the bauxite residues particles, which results in the precipitating of highly alkaline sodium-based salts [88]. Na₂CO₃, soda ash, nahcolite (NaHCO₃), and trona (Na₂CO₃.NaHCO₃.2H₂O) are examples of effloresced metals that have an adverse influence on the natural environment and human health [87,89,90]. The presence of effloresced minerals restricts the utilization of RM in building by decreasing the lifetime and durability of the material owing to crumbling and delamination. Also has an impact on the attractive appearance of construction materials containing RM [91,92].

Table 1
Worldwide bauxite production from 1970 to 2019 [64].

Country	Production Year (thousand metric tonnes)								
	1970	1980	1990	2000	2010	2016	2017	2018	2019
China	510	1750	3650	7950	36,830	66,150	68,390	68,390	68,410
Australia	9255	27,180	41,390	53,800	68,530	83,515	89,420	96,545	105,310
Brazil	500	4630	9750	14,380	32,030	39,245	38,120	32,005	32,005
Guinea	2610	13,910	16,150	17,990	17,630	32,425	51,700	59,575	63,230
Indonesia	1220	1249	1164	1151	27,410	1458	4400	10,500	10,500
India	1370	1780	4850	7560	12,660	24,220	22,775	23,230	26,050
Russia	NA	NA	NA	5000	5470	5430	5525	5655	5570
Jamaica	12,015	1198	10,960	11,125	8545	8545	8240	9965	9000
Kazakhstan	990	NA	NA	37,730	5315	4800	4845	6105	3810
Saudi Arabia	6	NA	NA	NA	NA	4465	3705	4325	4325
Guyana	3210	3050	1420	2690	1080	1480	1460	1925	2005
Vietnam	NA	NA	NA	16	80	1500	2700	3600	3600
Sierra Leone	450	670	1140	NA	1050	1370	1790	1940	2000
Others	NA	NA	NA	13,540	121,560	15,350	10,960	9230	9700
World	5725	93,270	115,010	138,890	228,800	289,970	314,040	332,985	345,535

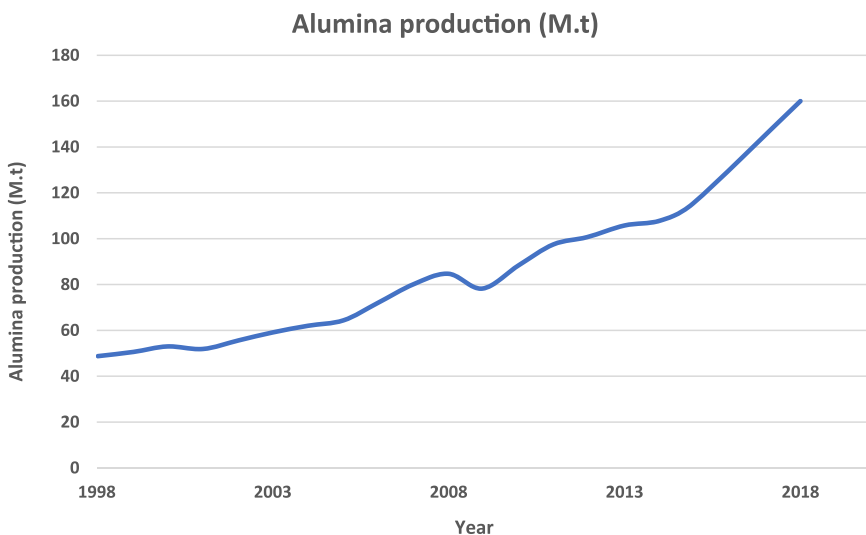


Fig. 2. Annual Al_2O_3 production worldwide [65].

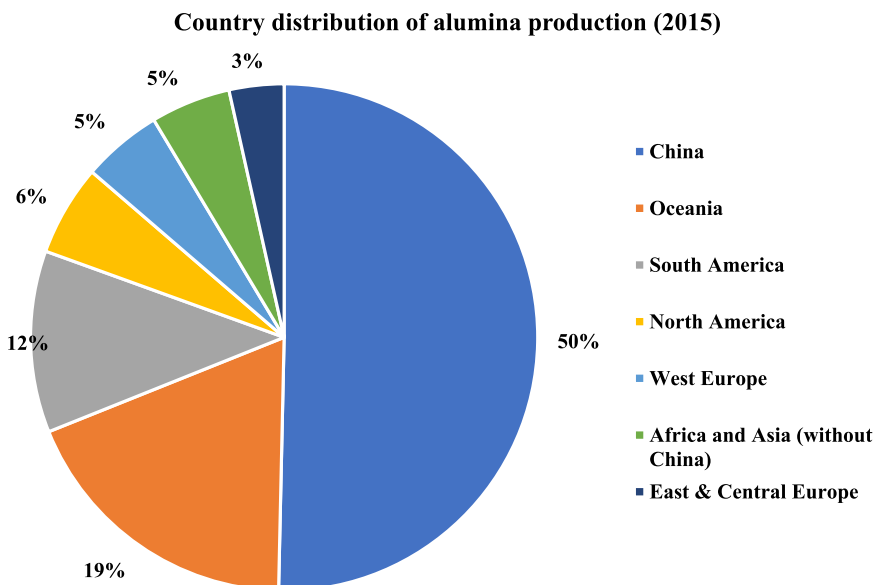


Fig. 3. Country distribution of Al_2O_3 production for 2015 [65].

Moreover, elevated sodium contents have been linked to plant development inhibition in soils polluted with RM. Also, RM leaking in aquatic environments degrades macroinvertebrate communities and reduces the penetration of light into the water column [93–95]. The elevated pH caused by RM pollution also hinders ammonia excretion in species of fish, resulting in ammonia storage and toxicity [96–100]. As a result, RM pollution impacts several trophic levels, having a significant impact on ecological biodiversity. The hazards involved with RM storage were demonstrated in 2010 when a containment wall collapsed in Ajka, Hungary. When approximately 1 million m^3 of bauxite residual slurry spilled out and inundated the adjacent land, a catastrophic ecological catastrophe ensued. Numerous human lives have been lost, and the surface waters and great swaths of land have been poisoned [101].

Apart from RM pollution of soils and waters, strong winds and dry weather accelerate dust emissions from bauxite residue dumpsites [88,102]. Pollution sources emissions pose a serious health danger in dry and warmer climates owing to the inhalation of caustic chemicals. Alkaline dust can induce throat and nose irritation, respiratory tract infections, and serious lung disorders with prolonged exposure [101]. The threats posed by RM were depicted in Fig. 6.

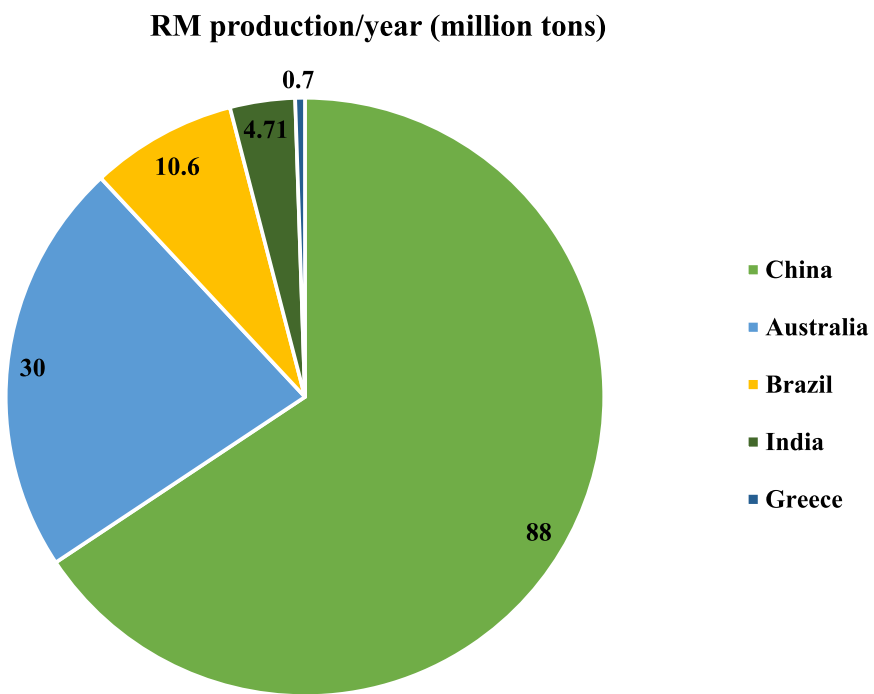


Fig. 4. The production of some countries for RM on an annual basis^[66–69] [1].

Table 2
Forms of bauxite ores in various regions [66,74].

Categorization	Country	Refs.
Gibbsitic	Australia, India, Ghana, Brazil, Jamaica, Guyana, Sierra Leone, Malaysia, Suriname, Guinea, Indonesia and Venezuela	[75,76]
Diasporic	Greece, China, Romania, and Turkey	
Boehmitic	Hungary, and Guinea	

5. Economic impacts of disposal of RM

Safe RM disposal is also economically challenging; it takes a significant amount of land: roughly 1 km² every five years for a 1 million ton/year Al₂O₃ factory [33], implying significant expenditures for the Al₂O₃ production industries. Additionally, RM-covered soil cannot be used for building or agriculture, even after the RM has dried [103]. The cost of safely disposing of RM is approximately 2% of the overall Al₂O₃ cost [33], but some reports claim 5% of the aluminum production value [104,105].

The average cost of Al₂O₃ in China, as per Shanghai Metal Market, is roughly 405 \$/ton of Al₂O₃ (Shanghai metal market), which is somewhat less than the \$ 440 stated by Sutar, Mishra, Sahoo and Maharana [67]. When one deems that RM disposal costs represent approximately 2% of the value of production [33] and the average price of Al₂O₃, the RM disposal cost is roughly 10 \$ per ton, which tends to make it prohibitively expensive and thus a financial strain on both aluminum manufacturing corporations and governments. The cost of properly disposing of RM in various countries is shown in Table 3.

The approach to overcoming ecological issues associated with RM disposal is the development of consumption technologies capable of consuming a considerable amount of red mud or converting it to a secondary resource [67,106]. Concrete is one of the composites that can consume large quantities of this RM by recycling it. Thus, reducing the environmental and economic burden to disposal of RM. One approach to recycling RM in concrete is to use it as a raw material to prepare the GP. What makes RM a strong candidate to be exploited with GPs is that it is highly alkaline and contains alumino-silicate s as indicated in the next paragraphs of this study.

6. Physical, chemical, and mineral properties of RM

RM is often gray-white to red in color, based on the quantity of iron oxide present. The melting point, density, and bulk density of RM are between 1100 and 1500 °C, 2700–2950 Kg/m³, and 750–1000 Kg/m³, respectively [14,44,107–109]. RM has a pH in the range of between 10 and 12.5, which is extremely alkaline. The liquid index of RM is 1.32–1.56 and the plasticity index is 17.2–30.5 [110,111].

The particle size distribution of RM is extremely fine. For example, Kumar and Kumar [36] used a laser particle size analyzer to

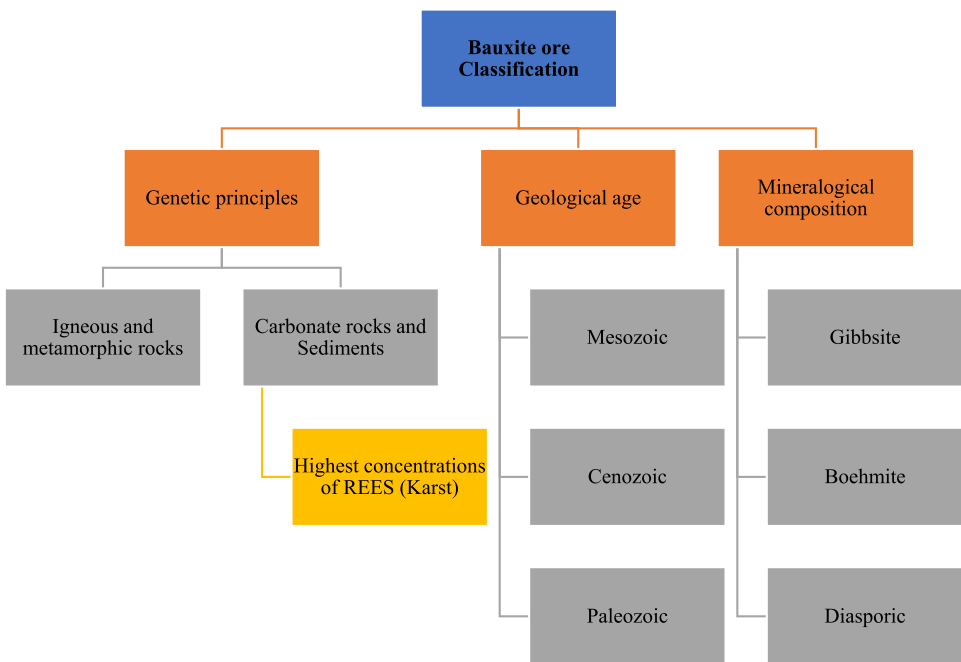


Fig. 5. A diagrammatic illustration of the categorization of bauxite ore [77].

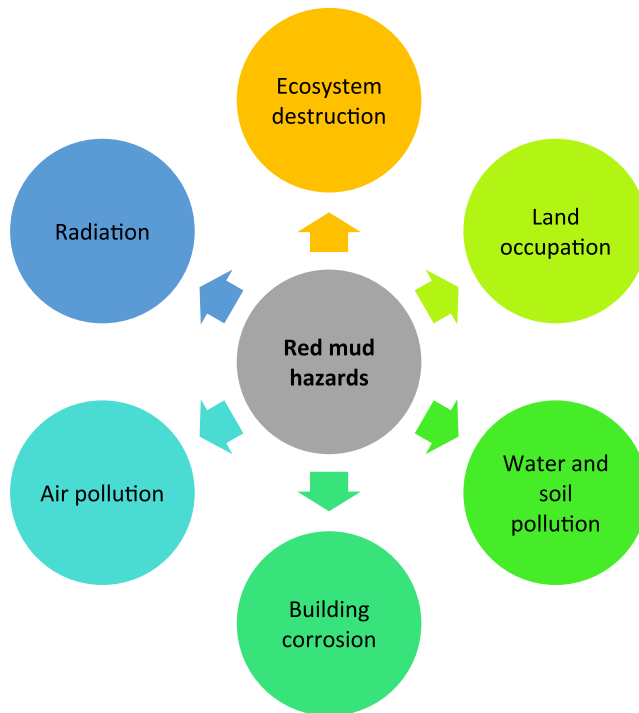


Fig. 6. Threats posed by RM.

determine the grain size distribution of red mud. Researchers discovered that the particle diameters X_{10} , X_{50} , and X_{90} of RM were 0.37, 1.57, and 56.88 μm , respectively, and that its particle size was significantly smaller and distribution was narrower than that of fly ash used in concrete. The specific surface area of RM is around $12\text{--}59 \text{ m}^2/\text{g}$, and the grain diameter ranges between 0.005 and 0.075 mm, with a porosity ratio substantially larger than that of ordinary soil [74,110,112]. As a result, RM exhibits excellent adsorption properties and is well suited for application as an adsorbent for heavy metals. For practical uses, the majority of study has focused on

Table 3
Costs associated with the safe disposal of RM in certain countries [66].

Country	RM production (M.t)/year	Safe disposal cost (million \$)/year
Greece	0.71	7.2
India	4.71	47.2
Brazil	10.5	107
Australia	30	302
China	89	885

the grain size and fineness of RM as a substitute for natural powder material. Fig. 7 shows the difference in the particle size distribution between RM and materials used in concrete such as slag, fly ash, and metakaolin. While Fig. 8 shows a comparison of the particles size distribution of RM in the Bayer process and sintering process. Although the majority of minerals in RM are liberated, various mineral particles prefer to stick to one another due to the ultra-fine particle size, resulting in a significant agglomeration occurrence among particles and the formation of aggregate-particles composed of various mineral particles [113].

Moreover, as a basic feature, the microstructure of RM has been extensively described using SEM, as illustrated in Fig. 9. Imaging indicates that RM is made of small particles ranging in size from a few to hundreds of microns. The varied forms of red dirt include spherical and flaky particles [114]. To compare with the mineral filler limestone powder, the specific surface area and pore size distribution of RM were evaluated. It is demonstrated that the surface area of RM was obviously greater than that of limestone powder at comparable particle size ratios. RM's porous character and large specific surface area lead to its adsorption capacity and interfacial adhesion behaviors.

Al_2O_3 , Fe_2O_3 , TiO_2 , SiO_2 , Na_2O , CaO , MgO , and K_2O are the major chemical ingredients of RM as shown in Fig. 10. Additionally, RM is frequently radioactive due to the presence of rare earth metals and trace amounts of uranium, thorium, and other radioactive elements [75,110,115–119]. Owing to regional variations in raw resources, Al_2O_3 manufacturing procedures, and technical advancements, the chemical composition of RM differs. The estimated chemical compositions of RM generated by the Bayer, sintering, and combination processes are presented in Table 4. In comparison to sintering RM, Bayer RM has a lower calcium and silicon concentration and a greater Al, Fe, and Na concentration. As shown in Table 4, the high iron RM is often Bayer RM. The worldwide high-iron RM's composition is analytically evaluated, as listed in Table 5.

The mineralogy of RM is complicated. In sintering RM, the major mineral stages include tricalcium aluminate, dicalcium silicate calcite, perovskite, and a trace of scattered iron-containing minerals and clay alumino-silicate minerals [37]. Regardless, there are primarily rare goethite (-FeO(OH)), hematite (Fe_2O_3), sodalite ($\text{Na}_2\text{OAl}_2\text{O}_3 \cdot 1.688\text{SiO}_2 \cdot 1.73\text{H}_2\text{O}$), opal ($\text{SiO}_2 \cdot n\text{H}_2\text{O}$), nepheline (3NaAlSiO_4 sodium hydroxide), rutile and anatase (TiO_2), gibbsite (aluminum hydroxide) [74,112,120].

7. RM applications

RM is created and is kept in the area where Bayer's process for recovering Al_2O_3 from bauxite ore is carried out. Nevertheless, recovery procedures often entail transporting RM to recovery units, such as those used in iron manufacturing, which will certainly raise expenses. As a result, procedures for using bauxite that may be implemented locally close to the bauxite production plant are ideal. Additionally, the recovery of metal values via pyrometallurgical mechanisms typically requires a large amount of energy. As a result, some 'green', ecologically friendly, and economically viable processes are required to recognize these values in RM. The process for developing such a comprehensive consumption of RM is represented in Fig. 11. The process involves a comprehensive characterization and selection of utilization processes, upon which a comprehensive utilization strategy is developed. By employing such a sophisticated method of RM use, valuable metals are recovered while also acquiring significant materials such as aluminum, iron, and alkali in the same processes, hence reducing expenses and waste. Additionally, approaches for utilizing the residues can be

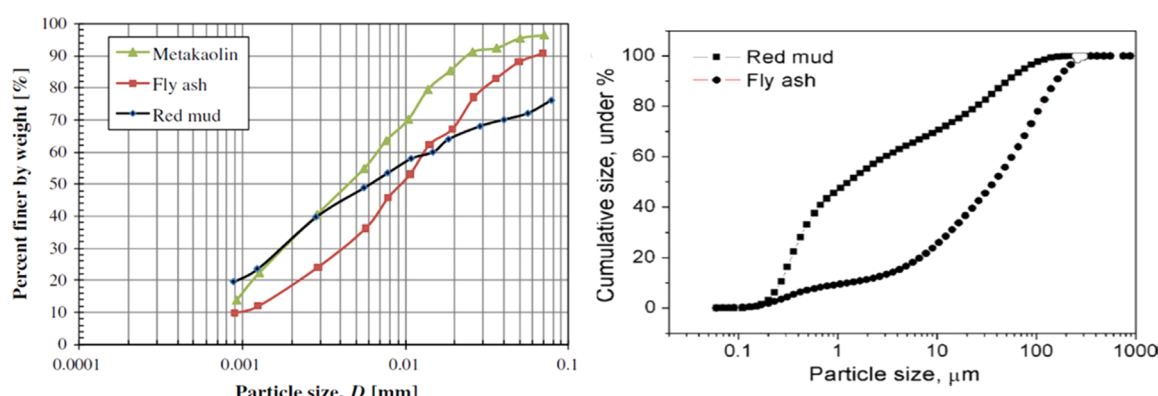


Fig. 7. Particle size distribution of RM, FA, and metakaolin [36,138].

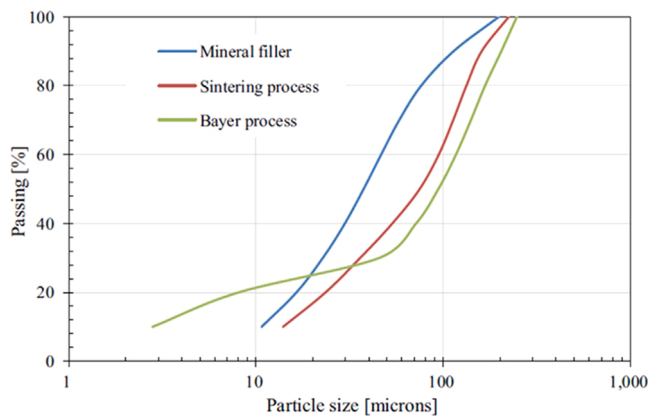


Fig. 8. Comparison of the particles size distribution of RM in the Bayer process and sintering process [126].

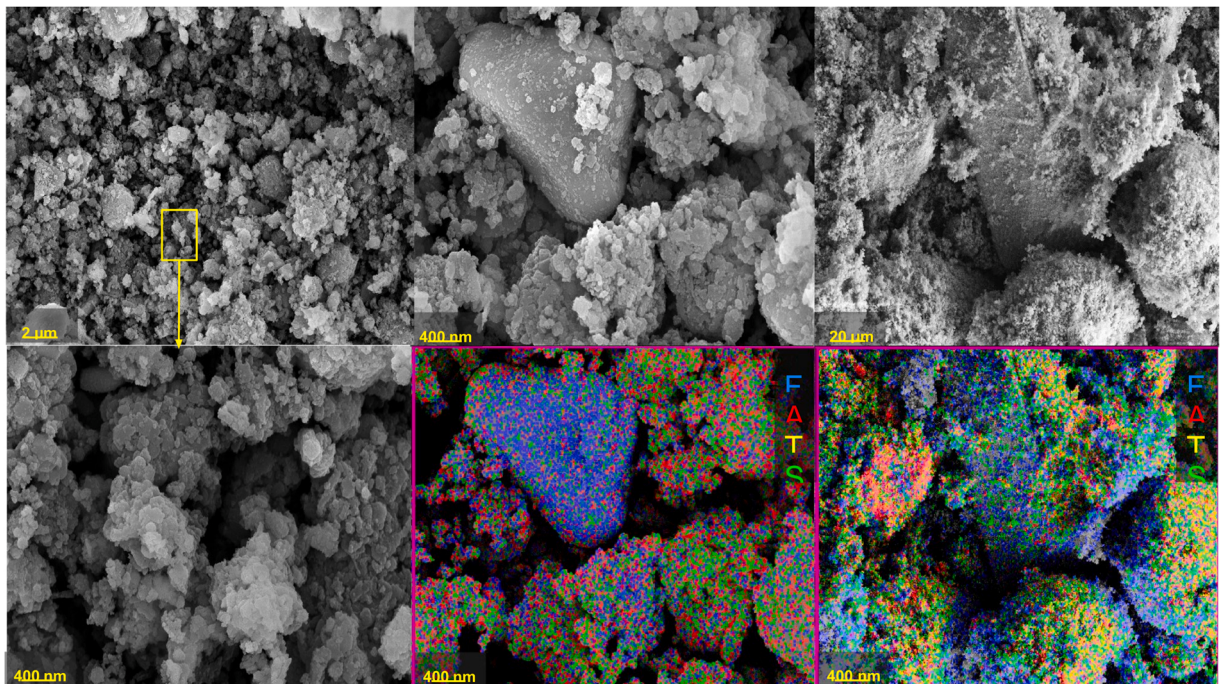


Fig. 9. SEM images of RM [139].

integrated into the process.[†]

Because of the many risks of environmental pollution connected with the direct disposal of RM [†]into the ecosystem, significant efforts have been made over the last few years to economically [†]reuse this waste. From 1964–2018, Figs. 12 and 13 depict the patent distribution and other [†]research efforts on RM usage in various fields. Amongst these, RM has been widely used as a [†]raw material in buildings, catalysts, wastewater treatment, and adsorbents. For instance, [†]HINDALCO, the world's largest aluminum producer, decided to commit to substituting RM [†]for the mined mineral used in cement clinker, aiming to consume 2.5 M.t annually from [†]the 4.5 M.t of by-product generated in its 3 refineries [141].

8. Geopolymer

A GP is an amorphous alkali-alumino-silicate [†] binder generated by reacting a source [†]material composed almost entirely of Al_2O_3 and SiO_2 [†] (for example, metakaolin) with an [†]alkaline medium (mostly alkali hydroxide/silicate) [144,145]. Once oversaturation is [†]attained, the raw material dissolves in an alkaline solution, generating Si and Al molecules that [†]produce gels. Subsequent restructuring and poly-condensation result in the creation of a stiff [†]three-dimensional network composed of Si^{4+}O_4 and Al^{3+}O_4 tetrahedrons linked by oxygen [†]bridges [146–150]. Alkali metal cations equalize the charge of Al^{3+} . Fig. 14 shows [†]in simplified form

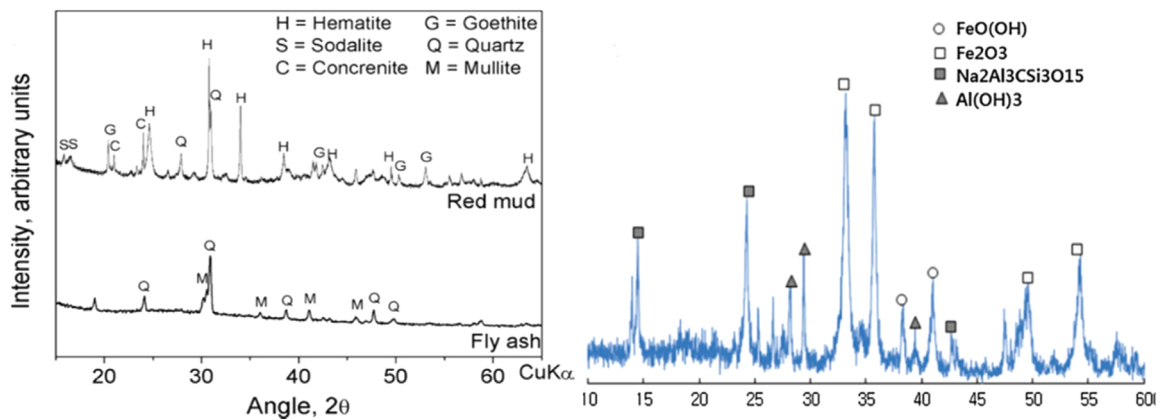


Fig. 10. Mineral components of RM [36,140].

Table 4

Chemical compositions of RM generated by the Bayer, sintering, and combination processes (wt%) [121].

RM Composition	Bayer RM	Sintering RM	Combination RM
Al ₂ O ₃	12–22	4–7	5.5–7.5
Fe ₂ O ₃	35–65	6–10	6.2–7.5
CaO	3–9	45–49	43.8–46.8
SiO ₂	4–20	22–23	20.2–20.5
K ₂ O	–	0.3–0.4	0.4–0.7
MgO	–	1.3–1.6	–
Na ₂ O	3–10	2.5–2.5	2.7–3.0
TiO ₂	0.2–10	2.6–3.0	6.2–7.7
LOI	12–16	7–10	–

Table 5

Chemical composition of RM by country.

Country	Chemical composition (wt%)						Refs
	Fe ₂ O ₃	Al ₂ O ₃	TiO ₂	SiO ₂	Na ₂ O	CaO	
America	55.5	12.10	4.6	4.55	5.2	–	[75]
Australia	36.25	17.15	3.95	23.85	1.65	3.95	[122]
	60.1	15.1	5.1	5.1	16.1	–	[123]
Brazil	45.5	15.2	4.25	15.5	7.0	1.16	[124]
China	31.25	18.50	6.20	8.30	3.25	18.1	[125]
	36.45	25.10	6.05	16.90	12.25	1.55	[126]
Germany	44.9	16.2	12.33	5.4	5.22	4	[124]
Greece	45.57	15.66	7.08	6.95	3.25	14.85	[127]
India	54.85	14.85	3.75	6.45	4.85	2.55	[122]
	38.85	17.27	18.85	9.65	6.85	–	[128]
	36.25	16.60	17.15	8.30	6.1	1.45	[129]
	51.05	17.55	3.25	8.66	8.04	1.66	[130]
Indonesia	50.3	24.1	2.8	20.4	–	0.4	[131]
Italy	35.3	20.1	11.7	9.3	7.6	6.6	[132]
Jamaica	49.4	13.3	7.4	3.1	4.1	9.3	[122]
	45.35	18.85	6.45	4.35	1.55	3.15	[133]
Russia	49.8	12.7	4.66	8.8	3.4	9.4	[134]
Spain	37.1	12.1	20.05	9.2	5.2	6.05	[135]
Turkey	36.95	20.35	4.97	15.77	10.05	2.24	[136]
UK	46.01	20.05	5.1	20.1	8.5	1.5	[137]

the geopolymserisation process. RM is very alkaline and composed of alumino-silicate s, making it an ideal source for the creation of GPs.

RM has been successfully employed as a GP binder in conjunction with a variety of different mineral compounds, such as FA, rice husk ash, slag, municipal solid waste, metakaolin, arsenic sludge, and coal gangue [151–155]. This review paper emphasizes the properties of GPs composed of RM and slag. The next sections describe the many characteristics impacting RM-FAGP, including workability and setting time, mechanical characteristics, thermal behavior, microstructure, and durability.

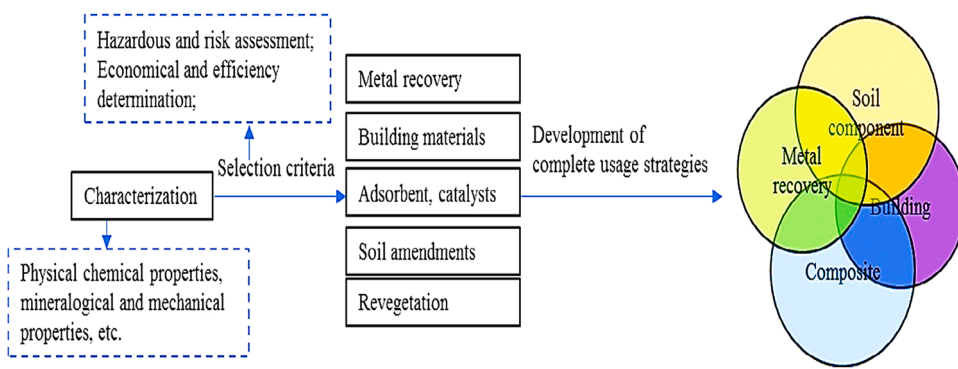


Fig. 11. Scheme of the development process for the full consumption of RM [142].

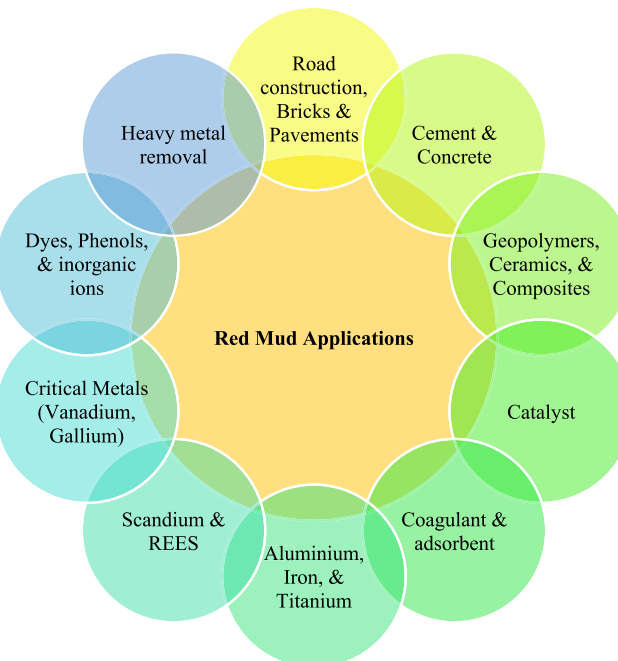


Fig. 12. RM application.

9. Properties of red mud-slag geopolymers

9.1. Fresh properties

Lemounga, Wang, Tang and Cui [157] and Bayat, Hassani and Yousefi [158] reported an improvement in the setting time of the GP and AA binder as the RM concentration rose, indicating that the RM operated as a retardant in the GP composites. The specimens with no RM had the shortest initial and final setting times. Bayat, Hassani and Yousefi [158] noticed that all specimens, except those comprising RM calcination temperature at 750 °C, had a much wider spread diameter than the OPC specimen. The samples containing RM that had been calcined at 750 °C was the only one that had a lower spread diameter than the OPC specimen, which was little affected by time. As the RM concentration of the mixture increased, the quick loss of consistency reduced resulting in a decrease in free calcium from slag. Consistency reduction was minimal in the samples with 40% RM. Hence, the inclusion of RM helped to decrease slump decline and stabilized the paste during the early blending hours. The AA slag-based sample exhibited the largest slump value, which reduced as RM rose and cohesiveness increased.

Zhang, Li, Li, Liu and Gao [159] observed a decrease in the fluidity of the RM-slag paste as the particles size of RM increased, as illustrated in Fig. 15. The specimens with the largest bulk particle size had the greatest fluidity, which was attributed to the superior particle size distribution in the GP paste. Bayat, Hassani and Yousefi [158] observed that as RM was added, the efflux time increased, resulting in a decrease in fluidity.

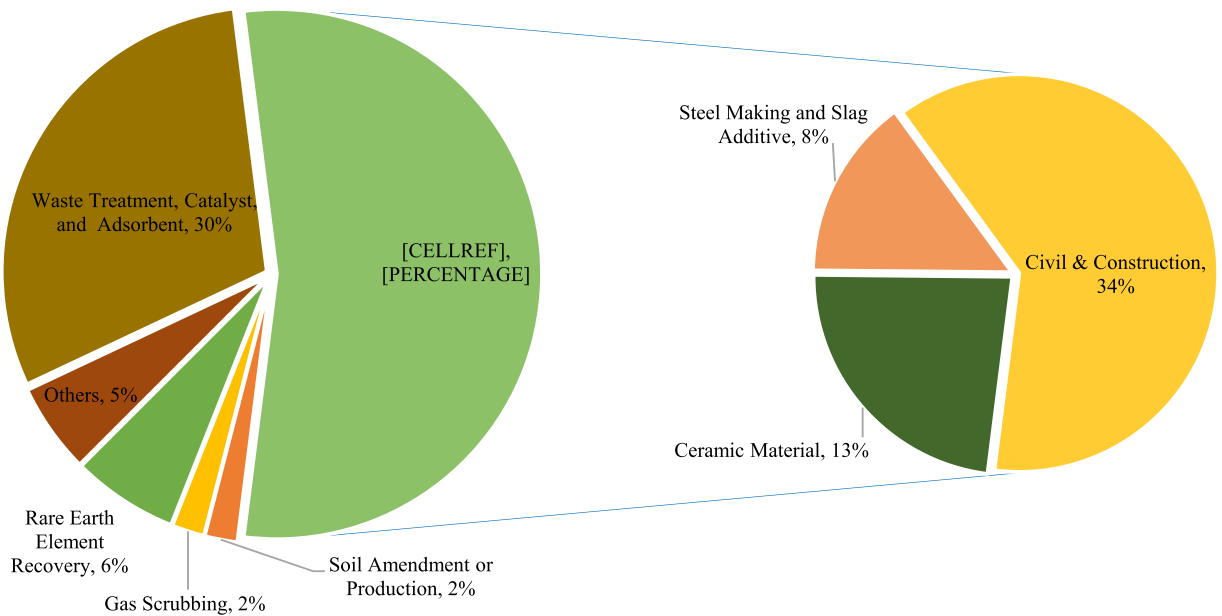


Fig. 13. RM utilization rate in various applications for the period from 1964 to 2018 [143].

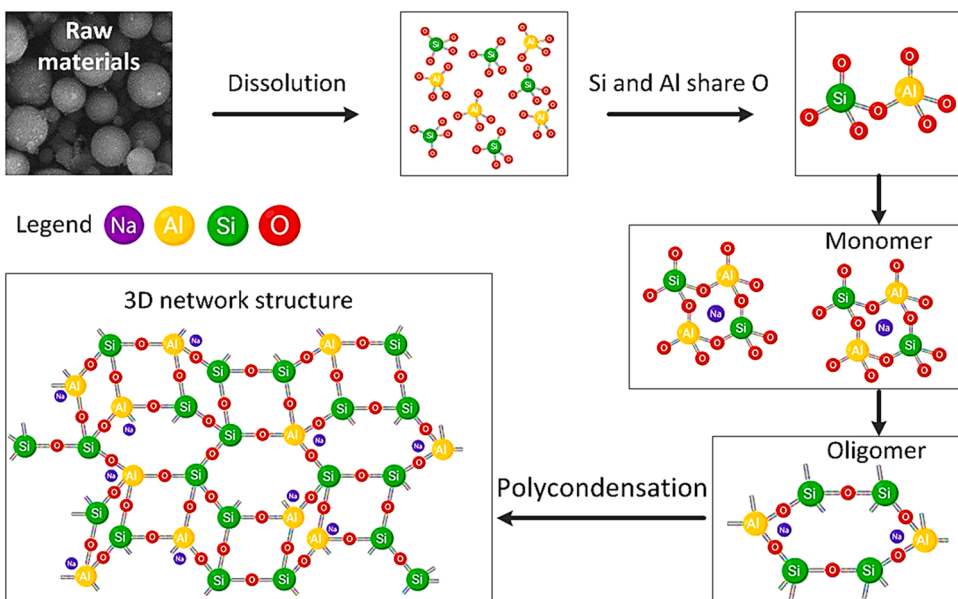


Fig. 14. Simplified geopolymisation process [156].

9.2. Setting time

The ratios of silica/alumina, liquid/solid, and $\text{Na}_2\text{O}/\text{Al}_2\text{O}_3$ of the GP composites all had an effect on the setting time of RM-GP.^r The setting time of an RM-SGP produced by Lemougna, Wang, Tang and Cui [157] was observed to be increased by up to 75% when the proportion of RM was raised as shown in Fig. 16. Although the setting time rose as the proportion of RM increased, the initial and final setting times were only 56 and 147 minutes, respectively, when 75% RM was used in an RM-SGP. Due to RM's lower reactivity than slag, it serves to retard the hardening process as the RM concentration increases and works as a setting time retardant in RM-SGP.^r

Pan, Li, Yu and Yang [160] investigated the setting characteristics of alkali-slag-red mud cement-based material (ASRC) in comparison to OPC 525. Initial and final setting times for a cement-based material containing 30% RM were determined to be 63 and 96 min, respectively. The ASRC material is set faster than 525 OPC. Therefore, the introduction RM-GP combination prolonged the

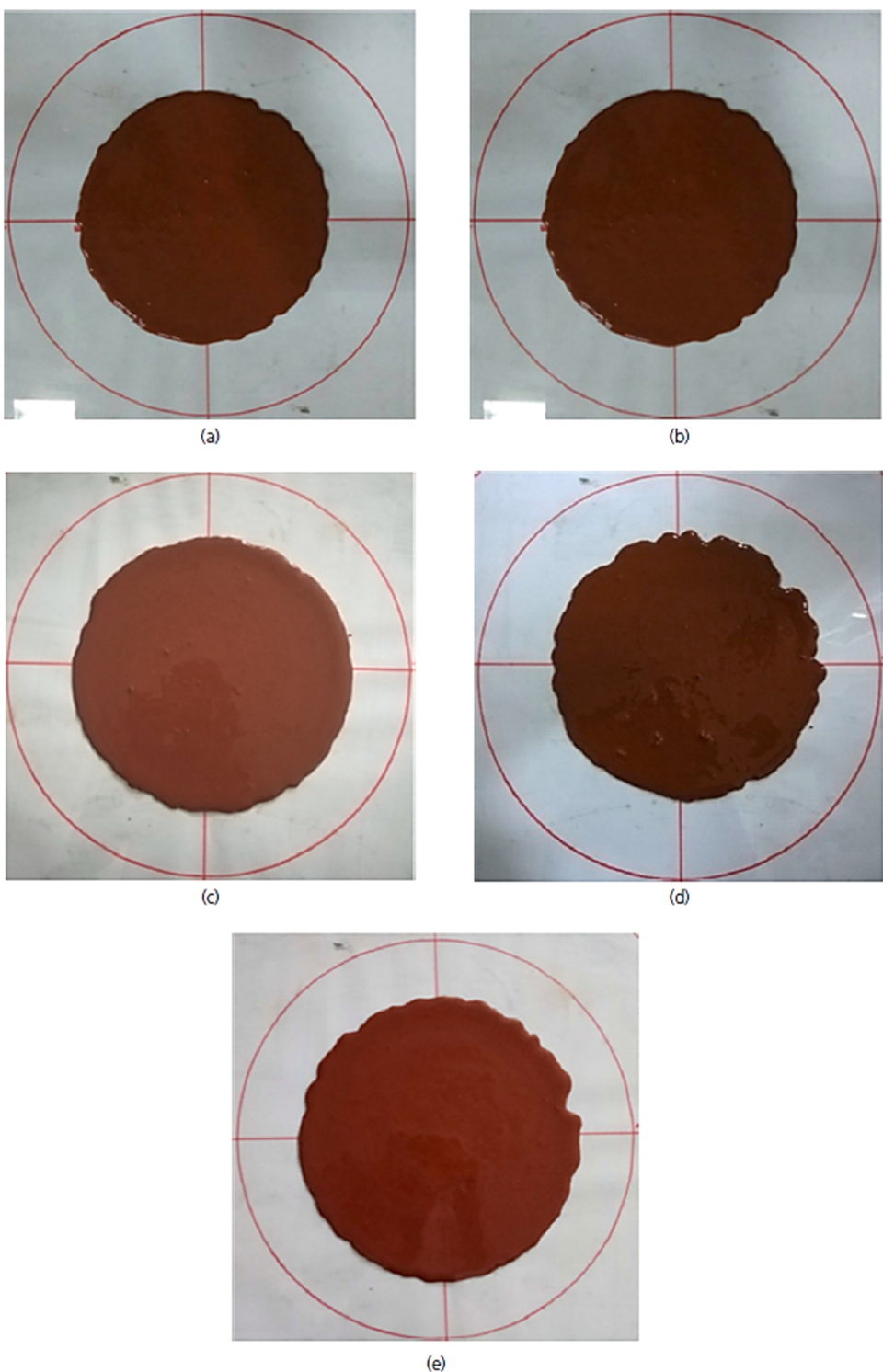


Fig. 15. Fluidity of RM-SGP: (a) RM-43; (b) RM-30; (c) RM-20; (d) RM-13; (e) RM-7 [159].

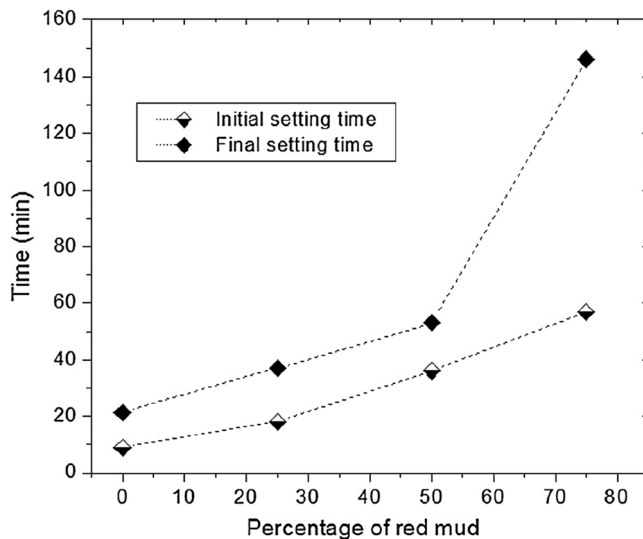


Fig. 16. Setting time of RM-SGP at 25 °C [157].

setting time. ↗.

9.3. Water absorption

The water absorption of the specimens synthesized with AA slag and RM increased as the RM ↗concentration increased, achieving values larger than those of the OPC specimens. Besides this, ↗as shown in Fig. 17, the investigators Kang and Kwon [140] observed an increase in the ↗moisture absorption coefficient as the amount of RM increased. Hyeok-Jung, Kang and Choe [161] observed ↗that increasing the RM inclusion improved the optimal moisture content, leading to a drop in the ↗highest dry unit weight. ↗Moreover, Singh, Aswath and Ranganath [162] conducted a water absorption experiment on the produced geopolymer bricks. The author discovered that increasing the RM concentration from 10% to 30% enhanced water absorption by 5%. When the RM content of the brick was raised from 30% to 50%, the increase in water absorption was more evident. Increased water absorption occurred not just as a result of the reaction with oxides, but also as a result of the looser matrix.

9.4. Mechanical properties

9.4.1. Impact of AA sols

Alkali hydroxides and alkali silicates seem to be the most often employed AAs in geopolymserisation procedures [53]. KOH or sodium hydroxide, as well as K_2SiO_3 or Na_2SiO_3 , are ↗commonly accessible and are utilized to make GPs. Si and Al ions are actively ↗dissolved from the alumino-silicate precursors in an alkaline medium. ↗

Pan, Li, Yu and Yang [160] created an ASRC that is composed of 30% RM and 70% slag and is activated ↗with solid water glass (8%

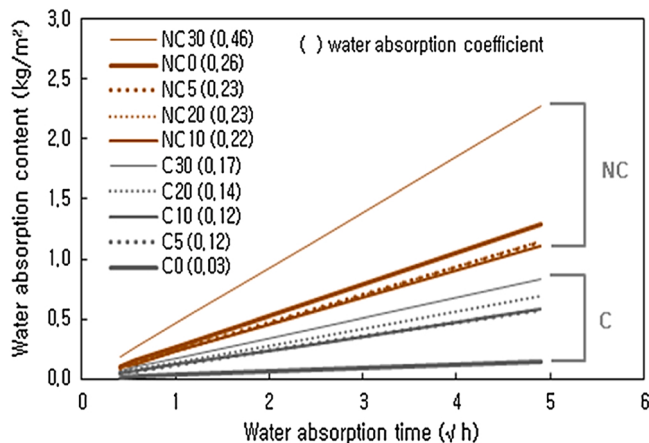


Fig. 17. Water absorption coefficient in binder OPC (C) and AA slag cement (NC) [140].

weight of binder) and sodium aluminate clinker (6% weight of binder). They evaluated the ASRC material's strength characteristics and resistance to the chemical attacks in comparison to a 525 OPC. The ASRC material's strength development was observed to be equivalent to that of OPC. After curing for 28-days, the ASRC materials obtained a higher compressive strength of 57 MPa. Flexural strength improved to a high of 9 MPa after curing for 28 days. Additionally, the materials had a low density, greater water required, a faster setting time, and resistance to carbonation, corrosion, and freeze-thaw cycles when comparison to OPC.

Lemougna, Wang, Tang and Cui [157] utilized solid sodium silicate and sodium hydroxide sol to produce an RM-SGP material in 25:75, 50:50, and 75:25 mixture proportions of slag and RM for use in lightweight and mortars materials. Compressive strength of the GP in 50:50 mixtures increased from 66–86 MPa under ambient temperature conditions when the silica modulus of the activator sol increased from 1.65 to an optimal value of 2, as shown in Fig. 18. Further than the optimal value, a decline in the strength of up to 61 MPa was observed. This is due to an overabundance of silicate inhibiting water evaporation and also creates the GP chain to disintegrate into separate monomers, lowering its strength. Moreover, Lin, Dai, Li and Sha [163] have developed high-performance, low-cost injectable materials from red mud, granular furnace slag (GBFS), and Class F fly ash to offer an ecologically responsible alternative to conventional grouting materials. Sodium hydroxide was utilized as an alkaline activator at concentrations ranging from 4% to 12%. The authors reported that the best mechanical property was obtained with a 6% NaOH solution concentration. However, it leaked a significant amount of water throughout the solidification process, compromising the slurry's stability and pumping effectiveness. When the concentration of NaOH solution is increased to 12%, the compressive strength increases only slightly from 3 to 28 days. It is shown that the excessively strong alkali environment inhibited compressive strength increase. As a result, the authors discovered that an 8% content of NaOH solution is best.

9.4.2. Impact of curing temperature and curing time

Pan, Li, Yu and Yang [160] reported a rising pattern in both the compressive and bending strengths of ASRC following 180 curing-days.

Lemougna, Wang, Tang and Cui [157] showed that an RM-SGP containing up to 50% RM can obtain compressive strengths of 50–60 MPa following 7-days of cure at 25 °C. When the proportion of RM was raised to 75%, a significant fall in 7 days strength to 11 MPa was observed. After 28-days of curing, the compressive strength of an RM-SGP containing 75% RM increased to 30 MPa. Hence, when RM is utilized in excess of 50%, a longer curing period of up to 28 days is necessary to produce a compressive strength of roughly 30 Mpa, as shown in Fig. 19. Furthermore, the compressive strength of the GP was shown to be affected by curing temperatures ranging from 20–65 °C. A GP content up to 50% RM demonstrated the highest strength of 86 MPa at 45 °C, whereupon the strength dropped. When RM content was risen to 75%, curing at a temperature of 45 °C was observed to be undesirable for compressive strength. However, when glass powder was substituted by 25% RM, the compressive strength increased with increased curing time and reaches a maximum value of 15 MPa after 3-days when cured at 65 °C for 1-, 2-, and 3-days, respectively, continued by curing at 25 °C for 7-days.

9.4.3. Impact of molar ratios of chemical compounds

Alkalinity (M_2O/H_2O) and silicate ratio or SiO_2/M_2O modulus (SiO_2/M_2O), where M=sodium, potassium, or calcium, are critical characteristics that aid in the geopolymserisation procedure. By raising the alkalinity (i.e., the M_2O / H_2O proportion), the dissolving or

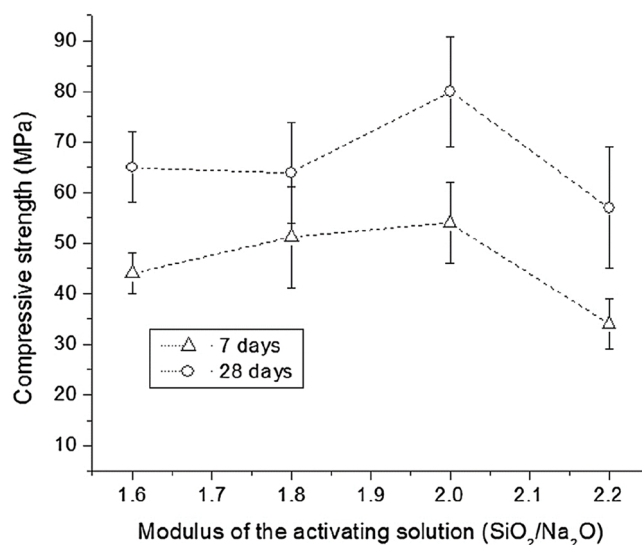


Fig. 18. Influence of the modulus of the activating sol on the 7 and 28-days compressive strength of GPs from 50% slag and 50% RM, cured at 25 °C [157].

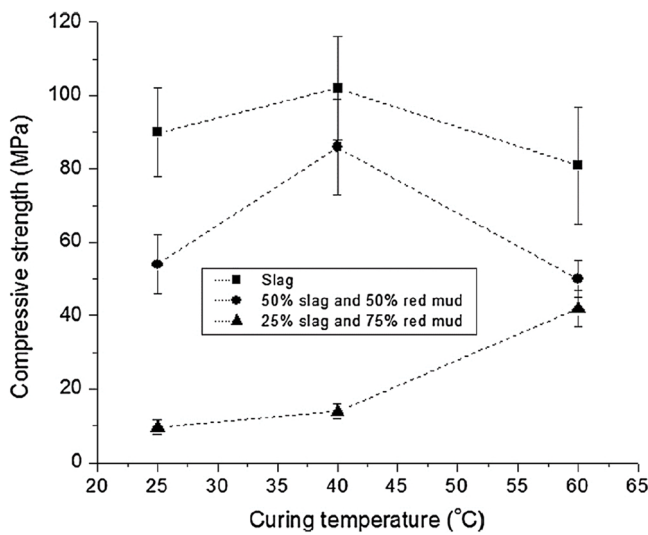


Fig. 19. Impact of temperature on the 7 and 28-days compressive strength of GPs from slag and slag/RM [157].

leaching of solid alumino-silicate molecules in an alkaline medium is accelerated. Likewise, raising the $\text{SiO}_2/\text{M}_2\text{O}$ ratio catalyzes the geopolymserisation processes and results in increased strength characteristics [164].

Compressive strength increased with increasing silica modulus from 1.3 to 1.7 for RM-SGP but thereafter dropped. The explanation for this was that an overabundance of silica inhibits the interactions of tetrahedral monomers, hence preventing the production of cyclic silicate molecules [165].

Lemouyna, Wang, Tang and Cui [157] included slag into a 50:50 mix ratio of red mud GP and reported a strength improvement from 66 MPa to 86 MPa under ambient curing conditions with a boost in $\text{SiO}_2/\text{M}_2\text{O}$ from 1.65 to 2.0. At an optimal silica modulus of 2, a lower $\text{SiO}_2/\text{M}_2\text{O}$ facilitates quicker reactivity during the early hydration phases resulting in higher strength.

Moreover, Singh, Aswath and Ranganath [28] utilized industrial wastes like fly ash and slag/micro-silica with sodium silicate solution and NaOH flakes for the mechanical activation of red mud. Slag by 10% wt. was used as an additive to geopolymers subjected to curing at ambient condition, whereas micro silica by 10% wt. was used for those geopolymers subjected to thermal curing. The compressive strength of red mud-fly ash geo-polymer with 30% red mud and 10% addition of slag, cured at ambient condition, decreased with the increasing amount of NaOH solution from 6 M to 10 M. Maximum compressive strength of 40.5 MPa at 6 M NaOH concentration was obtained. While thermally cured geopolymers samples with 10% addition of micro-silica required a higher NaOH concentration of 12 M to achieve a maximum compressive strength of 38 MPa.

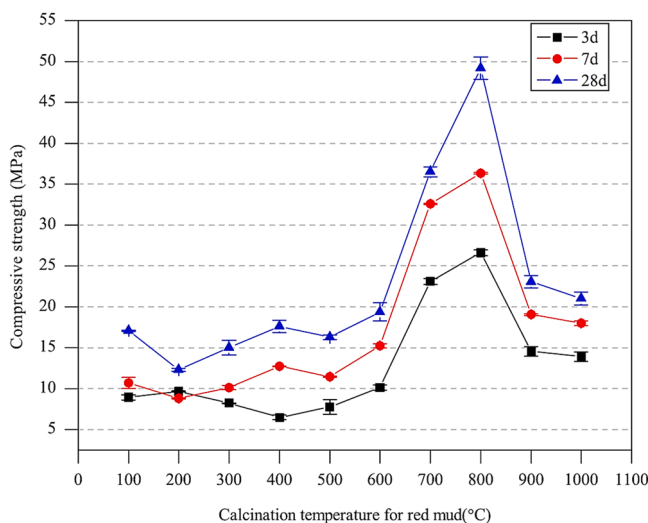


Fig. 20. Compressive strength of the binders versus the RM calcination temperature [165].

9.4.4. Impact of $\text{NaOH}/\text{Na}_2\text{SiO}_3$ ratio

In general, a blend of alkali silicate and alkali hydroxide is recommended for GP production, mostly to offset the disadvantages of alkali hydroxide activating. Alkali hydroxide activators are caustic in origin and produce enormous quantities of heat when alumino-silicate minerals are dissolved. Hence, in addition to Na_2SiO_3 , NaOH is frequently utilized in varied weight proportions for AA, which enhances the interaction between alkali sol and ingredients.^r

Cheng, Long, Zhang, Gao, Yu, Mei, Zhang, Guo and Chen [166] produced a slag-based cementitious material (SRCM) that was activated with Na_2SiO_3 and NaOH . Investigators used a $\text{NaOH} : \text{Na}_2\text{SiO}_3$ proportion of 1:3 for SRCM composed of 70% slag and 30% RM, which favored alumina dissolving and resulted in improved efficiency and outstanding compressive strength of around 16.7 MPa after 28-days.^r

9.4.5. Impact of calcination temperature

Owing to the reduced reaction of RM in its natural condition, it is often employed following thermal pre-treatment or calcination at high temperatures for several hours. Calcination leads to activation of Si and Al molecules in RM and increases the efficiency with which Al_2O_3 and SiO_2 dissolve in an alkaline medium, resulting in higher compressive strength. At various temperature levels throughout calcination, the Ca, Al, and Fe-rich crystal stages found in RM undergo phase transition via dehydration, dihydroxylation, and carbonation. At varying temperatures, crystallized mineral stages disintegrate into new phases like sodium aluminum silicate, solid Al_2O_3 , alkali-rich nepheline, gehlenite crystalline phase, and other ambiguous forms [167]. Calcination with or without alkali was shown to be highly efficient in increasing the reactivity of raw RM and generating more amorphous and glassy stages.^r

Ye, Yang, Ke, Zhu, Li, Xiang, Wang, Li and Xiao [165] investigated the impact of calcination temperature on the compressive strength of a GP composed of GBFS and RM in a weight ratio of 5:5. Compressive strength increased from 18–49 MPa as the temperature was increased from 100 to 800 °C, as shown in Fig. 20. Thermal treatment or calcination at a variety of temperatures alters the minerals stages present in RM, resulting in the creation of new phases with increased solubility in an alkaline condition. Calcination of RM increased the solubility of alumino-silicates for active dissolving in alkaline sol, resulting in increased geopolymerisation. Calcination at 800 °C was determined to be the most efficient strategy for dissolving alumino-silicates and producing maximal compressive strength.^r

9.4.6. Impact of plasticizer

Zhang, Li, Li, Liu and Gao [159] investigated the workability and mechanical characteristics of RM-SGP grout substance using a variety of super-plasticizers, including polycarboxylate (SPC), aliphatic (SPA), and naphthalene-based super-plasticizers (SPN). SPC was shown to be more stable in an alkali sol than SPA and SPN. With the introduction of super-plasticizers at various water/binder proportions, the fluidity of the GP grouting substance improved. SPA and SPN demonstrated good performance in terms of increasing compressive strength and workability while simultaneously decreasing the water/binder proportions. SPC demonstrated poor stability and had a detrimental influence on the grout material's compressive strength.^r

9.4.7. Particle size fraction

Furthermore, the particle size fraction had an impact on the mechanical characteristics of the GP composed of RM. Both coarser and finer RM geopolymers exhibited superior mechanical characteristics [159]. Therefore, particle sizes may be classified according to desirable characteristics. The improved mechanical performance is due to the increased dissolving response of Si^{4+} and Al^{3+} by

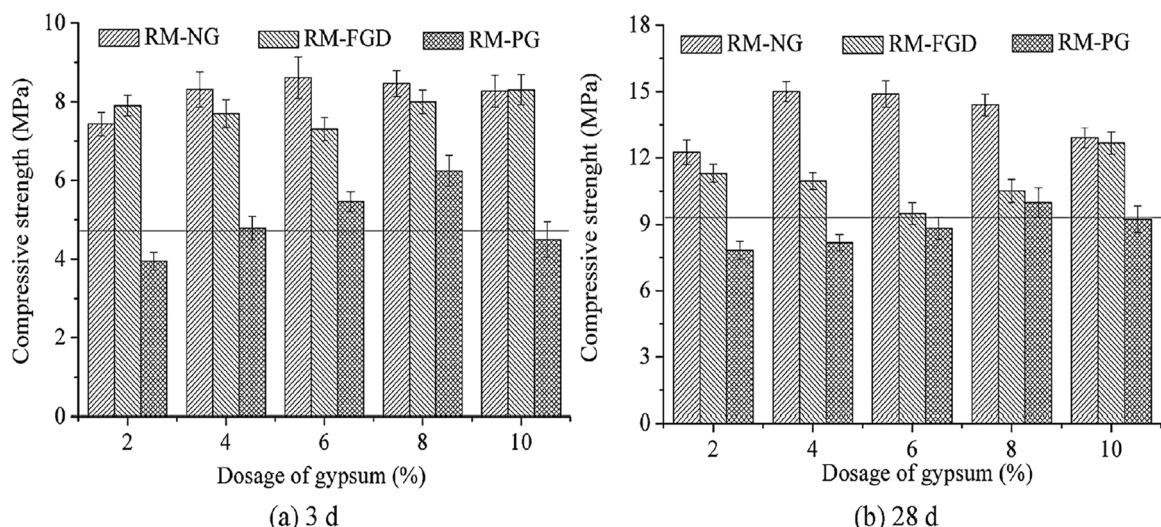


Fig. 21. Impact of various gypsums on the mechanical properties of RM-based grout paste (horizontal line in the figure is the compressive strength of control group) [168].

fine particles and the micro aggregate packing impact of coarser particles. As RM becomes finer, the Al_2O_3 , SiO_2 , and CaO concentrations drop dramatically, while the Na_2O and Fe_2O_3 concentrations slightly increase. Compressive strength was initially lowered and subsequently enhanced when the particle size percentage of RM rose.

9.4.8. Impact of additives

Li, Zhang, Li, Gao, Liu and Qi [168] studied the influence of incorporating several kinds of gypsum, including gypsum-dihydrate (NG), phospho-gypsum (PG), and flue gas desulfurization (FGD) gypsum, into RM-slag grout paste at various ratios, as shown in Fig. 21. The compressive strength of RM-slag grout after 3 and 28-days was found to be greatly increased with the addition of FGD and NG. There was no substantial increase in mechanical strength when RM-slag grout was mixed with phosphor-gypsum.

9.4.9. Impact of binder/fine Agg ratio

Lemouyna, Wang, Tang and Cui [157] produced a GP mortar using a slag-RM system. The compressive strength of mortar cured at 20 °C for 28 days was shown to decrease with a rise in sand concentration for all mixtures including 25%, 50%, and 75% RM as presented in Fig. 22. The insufficient interface connection between the GP matrix and the sand particles is the primary explanation for the compressive strength loss of the RM-SGP mortar. Nevertheless, the strength of the mortar was significantly affected by the concentration of slag at a content of up to 75%. Moreover, the possibility of using RM-SGP mortar in construction applications, particularly for low-cost constructions, was highlighted. Moreover, Singh, Aswath and Ranganath [162] synthesized geopolymers bricks using fly ash, red mud, and sand partially replaced by GBFS. Binder to aggregate ratios of 1:1 and 1:2 was considered. The sand was replaced by GBFS in 0, 20, 30%, 40% and 50%. The dry and wet compressive strength of geopolymers bricks with 10, 30 and 50% red mud was found to be reduced with increasing binder to aggregate ratio. The maximum dry and wet compressive strength for geopolymers brick without GBFS were 11.1 MPa and 9.5 MPa respectively obtained at 1:1 binder to aggregate ratio and 30% red mud content. Geopolymers brick with 50% RM as a binder and 50% GBFS as aggregate showed a higher strength of 15.5 MPa at a 1:1 binder to aggregate ratio. The geopolymers composite mortar was prepared using red mud, GGBS, and refuse mudstone with standard sand as the aggregate achieved a higher strength of 23.86 MPa at a binder to the aggregate ratio of 1:1, while refusing mudstone and alkali activator as the varying parameter.

9.5. Adsorption of heavy metals on the surface of the binders

Chen, Guo, Ding, Zhang, Xia, Wang and Zhou [169] investigated the adsorption rate of GPs to adsorption heavy metal ions. As shown in Fig. 23, the red dots in the spectrum scanning zone signified the adsorb of heavy metals (includes Pb, Cu, Cr, and Cd), whereas the gray dots indicated zero adsorption of heavy metals. As illustrated in Fig. 23, the ordering of adsorption capability for heavy metal ions was OPC-pervious concrete followed by GGBFS-GP-pervious concrete and RM-GP-pervious concrete. Besides, it was observed that the adsorption of heavy metal ions occurred primarily on the C-S-H gels. Moreover, heavy metal adsorption capability on the RM-GGBFS-based binder was in the sequence $\text{Cr}^{3+} < \text{Cu}^{2+} < \text{Cd}^{2+} < \text{Pb}^{2+}$. These findings indicated that the RM-GBFS-based binder might be utilized to build pervious concrete for prospective usage as a water filter.

9.6. Drying shrinkage

According to Bayat, Hassani and Yousefi [158], Bayat, Hassani and Azami [170], the values of drying shrinkage for specimens with 10% and 20% RM were 4.3 and 3.9 times larger than those for OPC specimens, respectively. The specimens 30% RM and 40% heat-treated RM increased by 10% in comparison to the sample that contains 0% RM. In comparison, as shown in Fig. 24, the drying shrinkage of a sample containing 40% heat-treated RM (at 750 °C) was reduced by 10% [34]. Lemouyna, Wang, Tang and Cui [157] observed a significant increase in the drying shrinkage of GPs as the RM concentration increased. Drying shrinkage was slowed early on with the introduction of RM. The introduction of RM at a concentration of up to 25% had no impact on the drying shrinkage values. In comparison, considerable shrinkage occurred in samples that contain 75% RM. Although the shrinkage of the 28-day-cured specimens was greater than the shrinkage of the OPC specimens, the inclusion of sand should reduce the drying shrinkage value, since sand does not shrink.

9.7. Thermal properties

Generally, geopolymers have better thermal stability and thermal insulation compared to conventional building materials. Geopolymers exhibit the least thermal expansion, lower thermal conductivity, and lower mass losses at higher temperatures than of ordinary Portland cement [171] and natural hydraulic lime-based mortar [172]. The thermal conductivity of geopolymers purely based on red mud was found to be 1.2035 W/m.K, which is lower relative to OPC with a thermal conductivity value of 1.206 [173]. The higher thermal conductivity of red mud geopolymers was due to the high iron content in RM. The blending of red mud with RHA in a 50:50 mix ratio resulted in the decrease in thermal conductivity value from 1.2035 to 0.4842 W/m.K. Ternary blended geopolymers containing red mud, RHA and diatomaceous earth showed better thermal properties in terms of thermal expansion at a temperature of 950 °C, whereas cement paste cannot withstand such a higher temperature as it may get damaged or broken. The thermal conductivity of alkali-activated slag-red mud composite was found to be 2.36% lower than that of cementitious composite, while thermal conductivity increased with the increase in red mud content from 0% to 20% and later decreased [170].

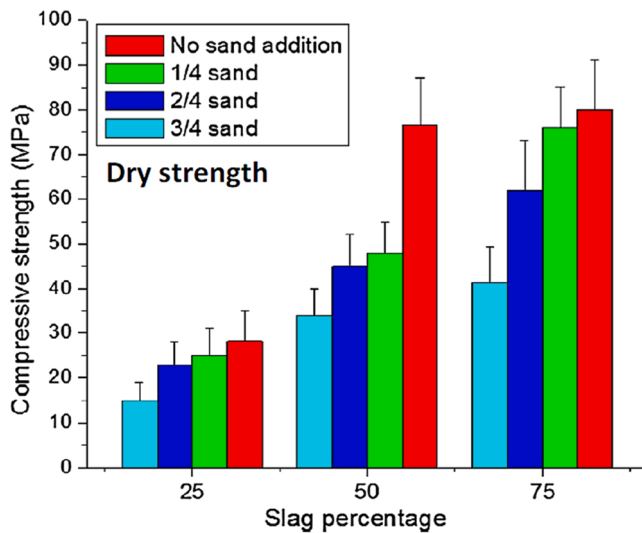


Fig. 22. 28-days compressive strength of RM-SGP composites cured at 25 °C [157].

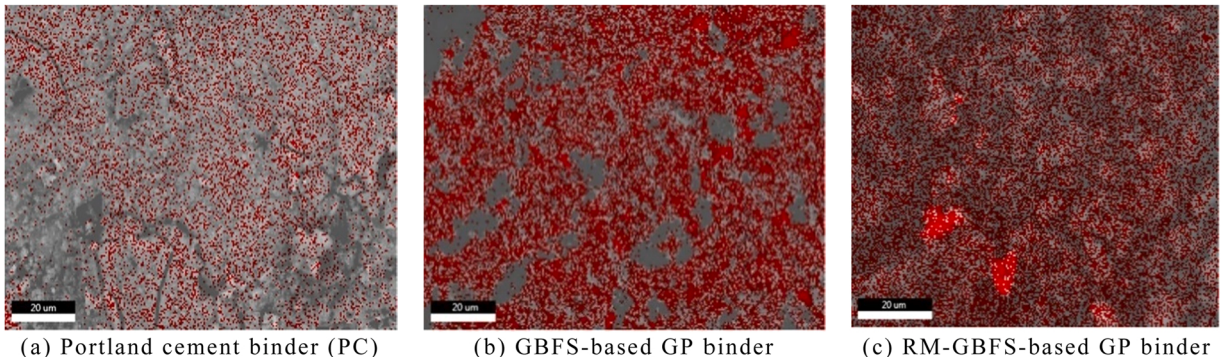


Fig. 23. Binder piece coated aggregate with EDS showing metal deposition after adsorption [169].

According to Bayat, Hassani and Yousefi [158], when the RM concentration grew from 0% to 40%, the specific heat raised from 815 J/(kg °C) to 860 J/(kg °C) as shown in Fig. 25. The thermal conductivity of the AA binder samples without RM was found to be 10% less than that of the OPC samples. Nevertheless, thermal conductivity increased with a rise in RM inclusion, which was attributable to the increased dosage of metal components such as Ti, Fe, and Al and in the paste area.

9.8. Microstructural properties

9.8.1. XRD

Krivenko, Kovalchuk, Pasko, Croymans, Hult, Lutter, Vandevenne, Schreurs and Schroeyers [174] investigated the X-ray phase diffraction patterns of RM-slag AA binders produced with sodium metasilicate and discovered the minerals lawsonite and klinop-ferrosilite. When the RM GGBS concentration was raised from 50% to 70%, the structure development process was retarded, implying that RM was only partially involved in the hydration of cement mechanisms. This result was made because the peaks of the raw RM specimens were also apparent in binders containing 30% RM and were more prominent when the RM concentration has risen to 50%. According to Bayat, Hassani and Azami [170], the sole crystallized molecule found in RM but not in the AA binder mixture was katoite, which had a peak centered around 13. The katoite in the sol was dissolved by the inclusion of an AA, which increased the pH of the mixture to 13.5. silicate and aluminum generated from the slag surfaces ought to have interacted with the calcium dissolved from the surface to produce more C-A-S-H gel. Zhang, Li, Li, Liu and Gao [159] reported that irrespective of the particle content of RM, all specimen's XRD analysis revealed the same phase composition, shown in Fig. 26. Moreover, according to Singh, Aswath and Ranganath [28], SEM images of unprocessed RM revealed clusters of hematite crystals forming agglomerates with diameters ranging from 1 to 5 m. In comparison, powdered RM samples lacked huge cohesive lumps. Transmission electron microscopy (TEM) pictures revealed that following pulverization, the crystal diameters of the phases in RM reduced. The pulverized sample exhibited an increased d spacing between the two crystalline planes as determined by high-resolution transmission electron

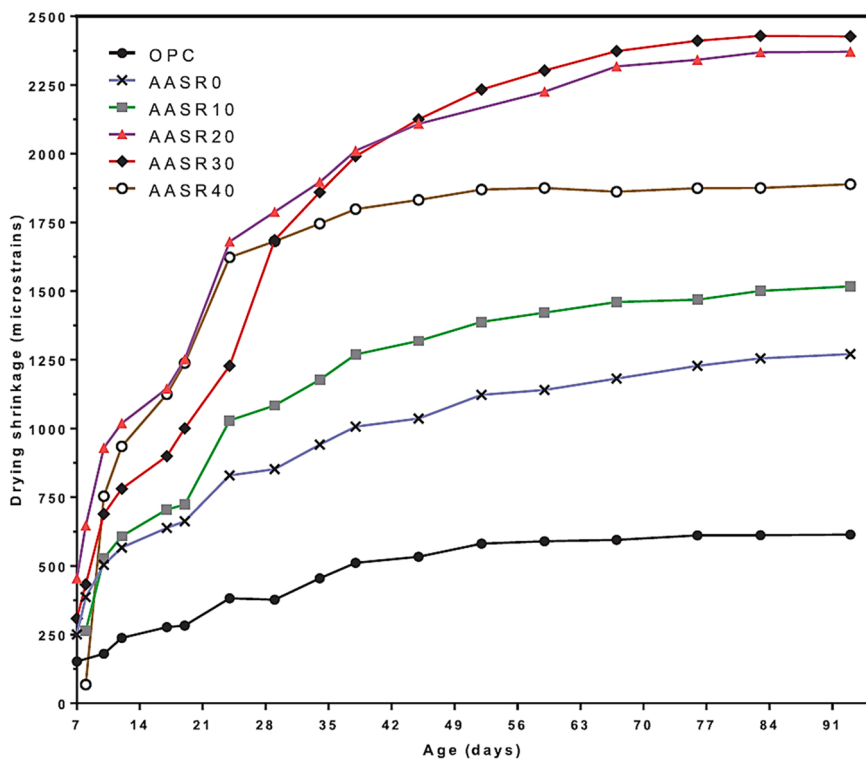


Fig. 24. Drying shrinkage of AA slag R and OPC concretes versus time [170].

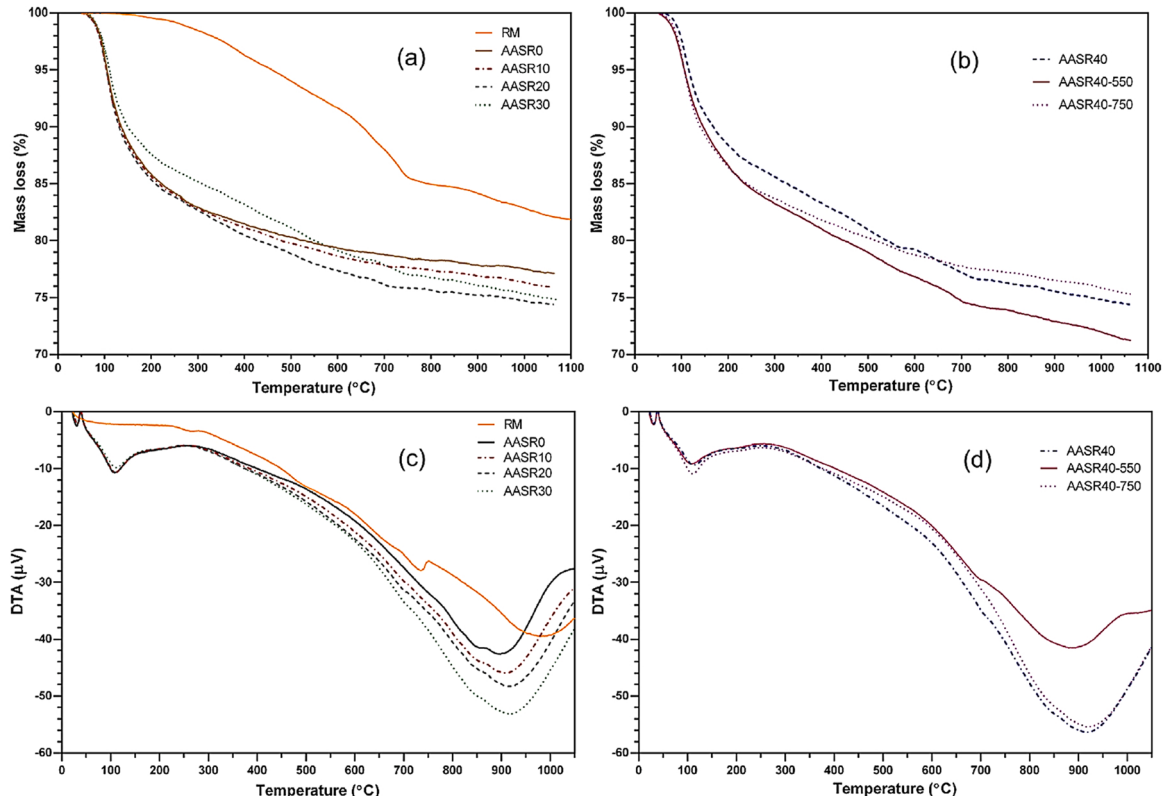


Fig. 25. Thermal analysis of the AA slag R paste of (a and b) TGA and (c and d) DTA [158].

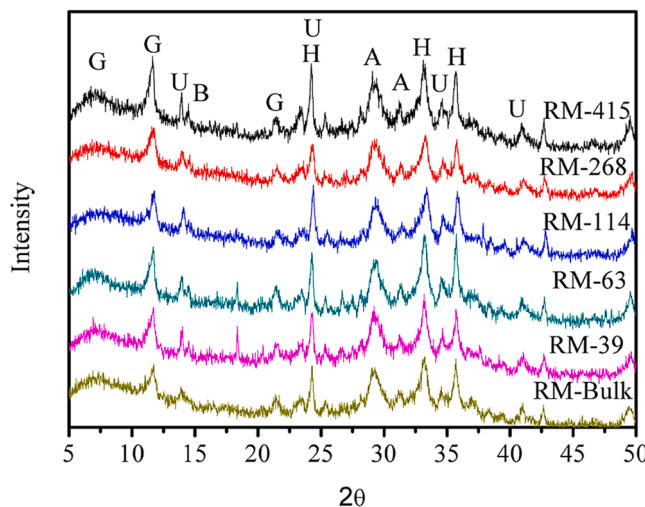


Fig. 26. XRD analysis of RM-GP with different RM fractions. (B-Calcite, C-Cancrinite, E-Sodalite, H-Hematite, S-Calcium silicate hydrate, Z-Un-named zeolite) [159].

microscopy (HRTEM). The ions were brighter, suggesting that their crystallinity had increased. The SAED imaging findings revealed an increase in the crystallinity of a few phases in the treated RM, which was verified to be hematite using HRTEM and XRD. The sample without RM included a few unreacted FA particles, which were significantly decreased in the sample with 10% RM. This was due to the increased degree of geopolymserisation caused by the addition of RM. Meanwhile, the sample containing 30% RM and a 10 M activator exhibited a thick matrix with some unreacted particles. ↗

9.8.2. SEM

Chen, Guo, Ding, Zhang, Xia, Wang and Zhou [169] investigated the SEM images of OPC, GGBS-GP, and RM-GGBS-GP. ↗Although the RM-GGBS-GP was as dense as the GGBS-GP, the former exhibited minor flaws ↗owing to un-reacted RM. The previous concrete or binder's ability to adsorb heavy metal ions got ↗greater as the RM concentration rose. The reduction in mechanical strength observed as RM ↗concentration increases were attributed to the rise in 2 stages. The first stage consisted of fine ↗circular particles less than 4 μm in diameter. The EDS analysis of this location revealed a ↗significant iron content, confirming the existence of hematite. The EDX analysis of the second ↗region revealed a larger content of Si, Ca, O, Al, and Na, indicating un-reacted slag, ↗resulting in a nonuniform GP microstructure and a decrease in the gel/space ratio [158,170].

Zhang, Li, Li, Liu and Gao [159] investigated the shape of hydration products with varying RM ↗percentages, as illustrated in Fig. 27. Due to the significant dissolving rates of Al^{3+} and Si^{4+} , ↗GP specimens comprising smaller particles of RM exhibited a compact microstructure. ↗Furthermore, the production of Na^+ was enhanced in the finer particles that acted as a charging ↗balancer in $[\text{AlO}_4]$. The SEM-EDS examination of the produced hydration products revealed ↗that the zone depicted was entirely composed of C-N-S-A-H gels of varying crystallization and ↗structure. ↗

9.9. Life cycle assessment

Before claiming a procedure is sustainable or environmentally friendly, it is necessary to ↗conduct a life cycle evaluation to determine the possible ecological impact of proposed ↗valorization methods and products. ↗

Jamieson, McLellan, Van Riessen and Nikraz [175] evaluated in comparison the embodied energies of Bayer liquor- derivative ↗GPs and OPC utilizing available studies and industry data. A concrete blend design using ↗17% binders (i.e., 9.3% FA, 3.9% wasted liquor, 0.2% lime, and 3.6% SiO_2 ↗fume) and 50% coarse and 33% sand particles were contrasted to a normal concrete mixture ↗with 17% OPC and the same volume of aggregates. Alternative additions, like plasticizers, ↗were ruled out owing to their low environmental impacts. Furthermore, it was believed that the ↗logistic parameters for OPC and GP manufacture are the same. The power calculations for ↗conventional OPC concrete comprised the extraction of raw resources, the whole manufacturing ↗process, and concrete manufacture. The more complicated computation for the Bayer- derivatized ↗GP concretes included the manufacture of sodium hydroxide, bauxite extraction, and ↗ Al_2O_3 ↗with hydrate synthesis, as well as treatment, and equaled 3.55 GJ/t. The power inputs of ↗ordinary Portland concrete were almost 3 times that of liquid GP concrete, at 1.01 GJ/t. When only ↗the binder was considered, the embodied energy of the RM-derivatized GP was less than a ↗quarter of that of the OPC binders. The reality that the liquor is deemed a toxic waste reduces ↗its embodied energy to zero (because the impurities loads must be eliminated to maintain the ↗ Al_2O_3 ↗character), resulting in even reduced embodied powers of roughly 0.28 Gt/J for the ↗GP binder. ↗

Jamieson, Penna, Van Riessen and Nikraz [176] have computed the energy inputs of a Bayer liquor activated GP ↗aggregates from fly ash (in a 50:50 blend with sand) to be 0.24 GJ/t, which is comparable to the ↗energy inputs of other aggregates like gravel (0.3 GJ/t). ↗

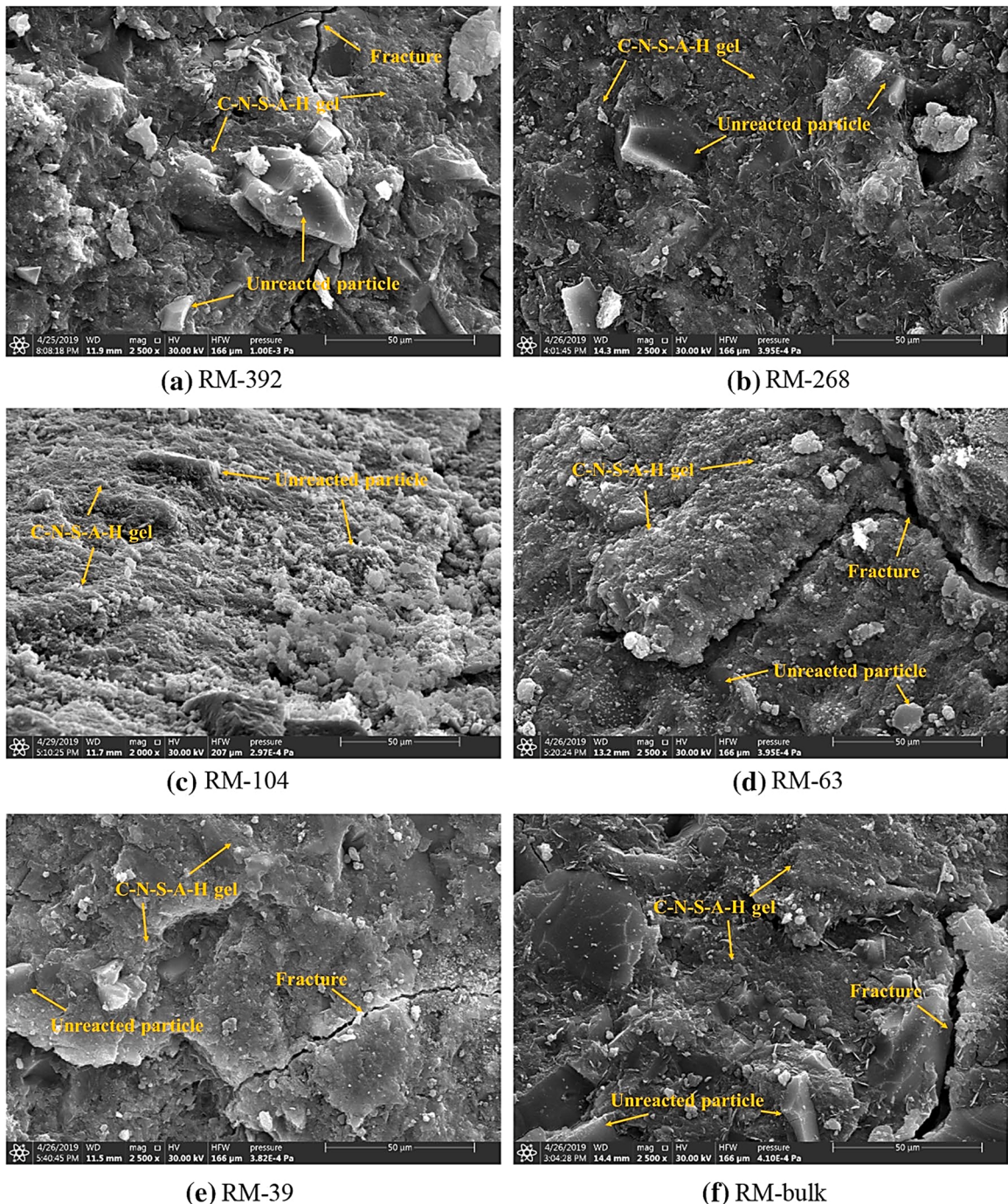


Fig. 27. SEM images of RM-SGP with different RM fractions [159].

In general, the influence of the production of the AA and alternate activators for AA materials is a significant issue to consider. Besides, the usage of spent Bayer liquor, RM slurry filtrate, and RM slurry [177–179].

9.10. Naturally occurring radioactive material (NORM)

Another critical factor to evaluate is the NORM concentration of RM, which has an impact on its suitability for usage in construction materials. Although NORM concentrations in RM are generally considered to be low [180,181], variances exist based on the source of the bauxite and the treatment factors. The investigations of Nuccetelli, Pontikes, Leonardi and Trevisi [182], and

Schroeyers, Sas, Bator, Trevisi, Nuccetelli, Leonardi, Schreurs and Kovacs [183] provide a comprehensive analysis of the NORM content of various RMs globally (2018). ↗

Two major concerns correlated with the accumulation of naturally occurring radio-nuclides in RM ↗are direct radon inhalation and external exposure to gamma radiation [184]. To assess ↗the potential application of RM-containing AA materials, the impact of the content of naturally ↗occurring radio-nuclides in the goods should be determined, for example, utilizing gamma ↗spectroscopic and compared to regulatory criteria. For example, the European Union's most ↗current directive on the maximum permissible concentration of NORM in construction materials [185] is based on the computation of the activity concentration indexes (according to ACI) as a gamma ↗dose estimating method utilizing observed activity contents of ^{226}Ra , ^{232}Th , and ^{40}K . If the ↗ACI value is less than the parameter of 1, the material can be utilized for construction purposes ↗without being radioactive. If the ACI of the RM-containing AA materials surpasses 1, a detailed ↗dosimetry analysis must be performed to ensure that the gamma dosage stays less than 1 mSv/y. ↗Because RM is included in the indicative listing of construction materials evaluated in terms of ↗gamma radiation that is emitted [185], it must also meet with the ACI when used as a ↗structural construction material element on its own. The yearly average concentration level of ↗ ^{222}Rn in a room should be less than 300 Bq/m³ for radon [185]. The quantities of naturally ↗occurring radio-nuclides in FAs used in construction materials in the European Union's ↗Member States are depicted in Fig. 28. While Table 6 summarizes the natural radionuclide of ↗RM in a number of member states of the European and other nations. ↗

The investigation by Krivenko, Kovalchuk, Pasko, Croymans, Hult, Lutter, Vandevenne, Schreurs and Schroeyers [174] included an evaluation of NORMs in alkaline ↗cementitious materials and concretes containing up to 90% RM from Ukraine. From the ^{238}U ↗set, the majority of radioactive elements were discovered at substantially greater quantities in RM ↗than in the utilized OPC and sand, however, with the exception of ^{210}Pb , all transuranic ↗elements were detected at somewhat elevated concentrations in blast furnace slag (BFS) than in RM. For the ↗ ^{232}Th series, the converse is true, with RM exhibiting significantly greater activity levels than ↗BFS, OPC, and sand. In comparison to RM, ^{40}K quantities were greater in OPC, BFS, ↗and sand. All types of cement and concretes had activity quantities below the applicable statutory limits for general and occupational exposures. ↗

Croymans, Schroeyers, Krivenko, Kovalchuk, Pasko, Marissens, Lutter and Schreurs [186] determined the activity concentrations of the ^{232}Th , ^{238}U , and ^{40}K ↗series in AA concrete containing up to 90% Ukrainian RM. We estimated quantity ↗indexes for public exposure produced by the utilize of concretes in construction materials, ↗roadways, and playgrounds, as well as workers exposed for construction practitioners. While the ↗concentration level indicators for public exposure rose as the RM concentration rises, even the ↗highest RM levels fell below the critical threshold of 1. The workers exposed to construction ↗projects employees surpassed the dosage of 0.3 mSv⁻¹ when concretes comprising more than 75 wt% ↗RM were used, however, the effective dose for highway construction workers was less than this ↗threshold even when concretes comprising 90 wt% RM were used. ↗

In general, all researchers concur that radioisotope concentration should be determined on an ↗individual level, depending upon the nature of RM employed and the intended usage of RM-based ↗products. ↗

10. Conclusions

In this review paper, the use of ↗RM with slag to produce geopolymers composites is specifically ↗↗↗pointed out. The conclusions drawn are as follows: ↗

1. This study emphasizes utilizing a variety of methods and materials to efficiently ↗employ RM as ↗GP precursors. Moreover, RM geopolymers composites have ↗significant potential for use as a ↗building material

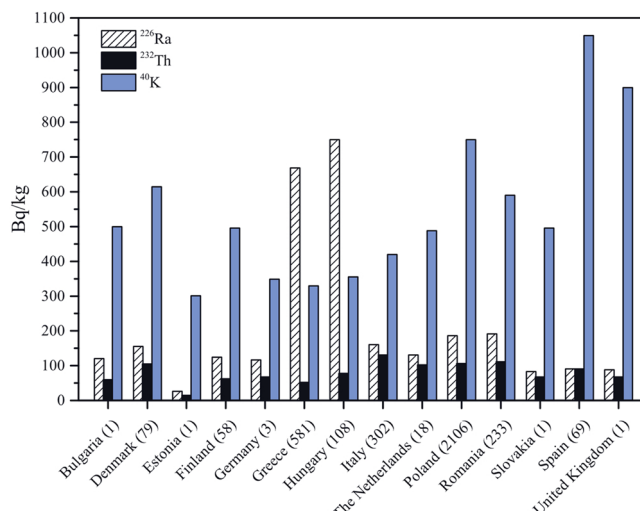


Fig. 28. Concentrations of naturally occurring radio-nuclides in FAs used in construction ↗materials in the European Union's Member States [182].

Table 6Natural radioactivity (Bq kg^{-1}) of RM in some countries [182].

Country	^{232}Th	^{226}Ra	^{40}K	Refs.
Australia	1128	325	30	[187]
	1355 ± 35	310 ± 20	350 ± 20	[188]
China	421 \pm 40	225 \pm 16	164 \pm 15	[189]
	705	476	154	[190]
	413 \pm 40	350 \pm 20	584 \pm 46	[189]
	555 \pm 55	477 \pm 25	400 \pm 33	[189]
	437 \pm 45	370 \pm 23	506 \pm 40	[189]
Brazil	350 \pm 18	138 \pm 2	45 \pm 1.8	[191]
Germany	184	123	—	[192]
Greece	344 \pm 34	233 \pm 46	45 \pm 13	[193]
	473 \pm 24	379 \pm 43	21 \pm 11	[194]
Hungary	400	255	—	[195]
	265	300	—	[195]
	284	348	49	[196]
Turkey	538 \pm 19	210 \pm 7	114 \pm 8	[197]
Italy	119	98	16	[198]
Jamaica	350	1047	336	[199]
	329	375	265	[199]

2. The utilization of RM for geopolymers addressed the need for an alternate method of properly disposing of RM, hence decreasing its negative impact on the environment. Furthermore, the expensive expense of the alkali activator solution was avoided by using RM due to its high NaOH content.
3. The GP specimens made with RM demonstrated excellent heavy metal adsorption. Moreover, it was discovered that the heavy metals were stable in the GPs produced, implying that GPs had a beneficial impact on the ecosystem.
4. The study of the influence of heat autoclave and treatment curing on GP specimens with varying curing regimes revealed excellent findings.
5. The use of calcined RM or alkali-thermally activated RM increased the amorphous structure of the RM particles, which aided in the production of GP gels.
6. The low reactivity of pure RM and its low $\text{SiO}_2/\text{Al}_2\text{O}_3$ ratio (often less than 2) are the key parameters preventing RM from being used effectively in geopolymers. As a result, RM must be combined with other alumino-silicate minerals that have a greater $\text{SiO}_2/\text{Al}_2\text{O}_3$ ratio.
7. All techniques of RM pre-activation, including alkali-thermal pre-treatment, calcination, mechanical co-grinding, and fine grinding or pulverization, resulted in improved mechanical and microstructure characteristics of the RM-GP.
8. When GP specimens are prepared using RM derived by flue gas desulfurization, a different AA is required than when GP specimens are prepared using raw RM.
9. Because the residual NaOH content of RM in relation to percent Na_2O ranges between 3 and 20.3%, it can be employed as a NaOH/AA source in geopolymers, thus lowering the cost of GP manufacturing.
10. The remaining sodium hydroxide in RM eliminates or significantly lowers the need for sodium hydroxide activator, permitting for acceptable strength to be achieved with sodium silicate sol as the sole AA.
11. The optimal AA content is determined by a number of criteria, including the type of the original source, chemical properties, pH, and $\text{SiO}_2/\text{Na}_2\text{O}$ and $\text{SiO}_2/\text{Al}_2\text{O}_3$ ratios. It is not essential for the strength of an RM-GP to rise proportionally with the alkaline content. Typically, RM-GPs include a $\text{Na}_2\text{SiO}_3:\text{NaOH}$ ratio of 2.5–3.
12. For applications requiring low strength, ambient curing on an RM-GP may be preferable. For improved durability and early-age strength, heat curing at temperatures between 60 and 80 °C may be beneficial.
13. Regarding radioisotopes, most researchers concur that radioisotope concentration should be determined on an individual level, depending upon the nature of RM employed and the intended usage of RM-based products.
14. On the other hand, regarding life cycle assessment, the influence of the production of the AA and alternate activators for AA materials is a significant issue to consider. Besides, the usage of spent Bayer liquor, RM slurry filtrate, and RM slurry.

11. Recommendations

Although the application of RM in building materials appears to be quite viable, significant issues remain for industrial application of GP produced utilizing RM, as follows:

1. There is a requirement to standardize the water/solid ratio in an attempt to implement it more accessible.
2. Due to the fact that the characteristics of RM vary depending on their source, treatment technique, and other parameters, it is difficult to generalize the GP characteristics produced.
3. Although the involvement of iron in the RM-GP formation has been highlighted, it requires more study.
4. Appropriate code standards are critical for applying diverse RM-GP applications.

5. Further study is required into the corrosion of steel reinforcement, bonding behavior, and structural behavior of reinforced RM-GP materials. ↗
6. Comprehensive research is required to enhance the physical and chemical characteristics of RM and GP by incorporating additives and optimizing the porous structure, such as Alccofine, nano silica, microfibers, quartz powder, bio-additives, epoxy-based composite, and nano-materials that have been successfully used in other forms of GP composites. ↗
7. Additional studies on the structural and durability characteristics of RM and GP are required before they may be used to remodel structures and precast products. ↗

Declaration of Competing Interest

The authors declare that they have no known competing financial interests or personal relationships that could have appeared to influence the work reported in this paper.

References

- [1] S.A. Yildizel, B.A. Tayeh, G. Calis, Experimental and modelling study of mixture design optimisation of glass fibre-reinforced concrete with combined utilisation of Taguchi and Extreme Vertices Design Techniques, *J. Mater. Res. Technol.* 9 (2) (2020) 2093–2106.
- [2] A.M. Zeyad, M.A.M. Johari, Y.R. Alharbi, A.A. Abadel, Y.M. Amran, B.A. Tayeh, A. Abutaleb, Influence of steam curing regimes on the properties of ultrafine POFA-based high-strength green concrete, *J. Build. Eng.* 38 (2021), 102204.
- [3] B.A. Tayeh, M.W. Hasaniyah, A.M. Zeyad, M.M. Awad, A. Alaskar, A.M. Mohamed, R. Alyousef, Durability and mechanical properties of seashell partially-replaced cement, *J. Build. Eng.* 31 (2020), 101328.
- [4] H.M. Hamada, A. Alya'a, F.M. Yahaya, K. Muthusamy, B.A. Tayeh, A.M. Humada, Effect of high-volume ultrafine palm oil fuel ash on the engineering and transport properties of concrete, *Case Stud. Constr. Mater.* 12 (2020), e00318.
- [5] A.S. Faried, S.A. Mostafa, B.A. Tayeh, T.A. Tawfik, The effect of using nano rice husk ash of different burning degrees on ultra-high-performance concrete properties, *Constr. Build. Mater.* 290 (2021), 123279.
- [6] M. Arafa, B.A. Tayeh, M. Alqedra, S. Shihada, H. Hanooona, Investigating the effect of sulfate attack on compressive strength of recycled aggregate concrete, *J. Eng. Res. Technol.* 4 (4) (2017).
- [7] M. Amin, A.M. Zeyad, B.A. Tayeh, I.S. Agwa, Effects of nano cotton stalk and palm leaf ashes on ultrahigh-performance concrete properties incorporating recycled concrete aggregates, *Constr. Build. Mater.* 302 (2021), 124196.
- [8] B.A. Tayeh, A. Hakamy, M. Amin, A.M. Zeyad, I.S. Agwa, Effect of air agent on mechanical properties and microstructure of lightweight geopolymer concrete under high temperature, *Case Stud. Constr. Mater.* (2022), e00951.
- [9] M.S. Saif, M.O. El-Hariri, A.I. Sarie-Eldin, B.A. Tayeh, M.F. Farag, Impact of Ca⁺ content and curing condition on durability performance of Metakaolin-based Geopolymer Mortars, *Case Stud. Constr. Mater.* (2022), e00922.
- [10] M. Amin, A.M. Zeyad, B.A. Tayeh, I.S. Agwa, Effect of high temperatures on mechanical, radiation attenuation and microstructure properties of heavyweight geopolymer concrete, *Struct. Eng. Mech.* 80 (2) (2021) 181–199.
- [11] S.M. Taher, S.T. Saadullah, J.H. Haido, B.A. Tayeh, Behavior of geopolymer concrete deep beams containing waste aggregate of glass and limestone as a partial replacement of natural sand, *Case Stud. Constr. Mater.* 15 (2021), e00744.
- [12] D. Yang, W. Deng, A. Tan, Z. Chu, W. Wei, R. Zheng, Y. Shangguan, A. Sasaki, M. Endo, H. Chen, Protonation stabilized high As/F mobility red mud for Pb/As polluted soil remediation, *J. Hazard. Mater.* 404 (2021), 124143.
- [13] I. Sevgili, Ö.F. Dilmaç, B. Şimşek, An environmentally sustainable way for effective water purification by adsorptive red mud cementitious composite cubes modified with bentonite and activated carbon, *Sep. Purif. Technol.* 274 (2021), 119115.
- [14] E. Atan, M. Sutcu, A.S. Cam, Combined effects of bayer process bauxite waste (red mud) and agricultural waste on technological properties of fired clay bricks, *J. Build. Eng.* 43 (2021), 103194.
- [15] A. Tolstoy, V. Lesovik, E. Glagolev, A. Krymova, Synergetics of hardening construction systems. IOP Conference Series: Materials Science and Engineering, IOP Publishing, 2018.
- [16] Y. Wang, D. Li, X. Liu, W. Zhang, Z. Li, Y. Li, Y. Ren, H. Li, Mechanism of magnetizing the Bayer red mud and meanwhile improving the cementitious activity of its tailings by using biomass, *J. Clean. Prod.* 287 (2021), 125016.
- [17] M. Lorena Figueiredo Martins, P. Roberto Ribeiro Soares Junior, T. Henrique da Silva, P. de Souza Maciel, I. Peixoto Pinheiro, A. Cesar da Silva Bezerra, Magnesium industry waste and red mud to eco-friendly ternary binder: producing more sustainable cementitious materials, *Constr. Build. Mater.* 310 (2021), 125172.
- [18] A.P. Sintsov, E.L. Shchesnyak, V.V. Galishnikova, R.S. Fediuk, N.A. Stashevskaya, Effect of nano-modified additives on properties of concrete mixtures during winter season, *Constr. Build. Mater.* 237 (2020), 117527.
- [19] C. Scribot, W. Maherzi, M. Benzerour, Y. Mamindy-Pajany, N.-E. Abriak, A laboratory-scale experimental investigation on the reuse of a modified red mud in ceramic materials production, *Constr. Build. Mater.* 163 (2018) 21–31.
- [20] G. Garau, M. Silvetti, S. Deiana, P. Deiana, P. Castaldi, Long-term influence of red mud on As mobility and soil physico-chemical and microbial parameters in a polluted sub-acidic soil, *J. Hazard. Mater.* 185 (2) (2011) 1241–1248.
- [21] G. Garau, P. Castaldi, L. Santona, P. Deiana, P. Melis, Influence of red mud, zeolite and lime on heavy metal immobilization, culturable heterotrophic microbial populations and enzyme activities in a contaminated soil, *Geoderma* 142 (1) (2007) 47–57.
- [22] Y. Hu, S. Liang, J. Yang, Y. Chen, N. Ye, Y. Ke, S. Tao, K. Xiao, J. Hu, H. Hou, W. Fan, S. Zhu, Y. Zhang, B. Xiao, Role of Fe species in geopolymer synthesized from alkali-thermal pretreated Fe-rich Bayer red mud, *Constr. Build. Mater.* 200 (2019) 398–407.
- [23] A.L. Almutairi, B.A. Tayeh, A. Adesina, H.F. Isleem, A.M. Zeyad, Potential applications of geopolymer concrete in construction: a review, *Case Stud. Constr. Mater.* 15 (2021), e00733.
- [24] S. Samal, A.K. Ray, A. Bandopadhyay, Proposal for resources, utilization and processes of red mud in India—a review, *Int. J. Miner. Process.* 118 (2013) 43–55.
- [25] F.A. Jawad Ahmad, Rebeca Martinez-Garcia, Jesús de-Prado-Gil, Shaker M.A. Qaidi, Ameni Brahmia, Effects of waste glass and waste marble on mechanical and durability performance of concrete, *Sci. Rep.* 11 (1) (2021) 21525.
- [26] A. Mansi, N.H. Sor, N. Hilal, S.M. Qaidi, The impact of nano clay on normal and high-performance concrete characteristics: a review. IOP Conference Series: Earth and Environmental Science, IOP Publishing, 2022.
- [27] T.-a Zhang, Y. Wang, G. Lu, Y. Liu, W. Zhang, Q. Zhao, Comprehensive utilization of red mud: current research status and a possible way forward for non-hazardous treatment. TMS Annual Meeting & Exhibition, Springer, 2018, pp. 135–141.
- [28] S. Singh, M. Aswath, R. Ranganath, Effect of mechanical activation of red mud on the strength of geopolymer binder, *Constr. Build. Mater.* 177 (2018) 91–101.
- [29] D. Pei, Y. Li, D. Cang, In situ XRD study on sintering mechanism of SiO₂-Al₂O₃-CaO-MgO ceramics from red mud, *Mater. Lett.* 240 (2019) 229–232.
- [30] Y. Li, X. Liu, Z. Li, Y. Ren, Y. Wang, W. Zhang, Preparation, characterization and application of red mud, fly ash and desulfurized gypsum based eco-friendly road base materials, *J. Clean. Prod.* 284 (2021), 124777.
- [31] Y. Guo, J. Li, K. Yan, L. Cao, F. Cheng, A prospective process for alumina extraction via the co-treatment of coal fly ash and bauxite red mud: investigation of the process, *Hydrometallurgy* 186 (2019) 98–104.

- [32] B. Mendes, I.K. Andrade, J.M. de Carvalho, L. Pedroti, A. de Oliveira Júnior, Assessment of mechanical and microstructural properties of geopolymers produced from metakaolin, silica fume, and red mud, *Int. J. Appl. Ceram. Technol.* 18 (1) (2021) 262–274.
- [33] P.E. Tsakiridis, S. Agatzini-Leonardou, P. Oustadakis, Red mud addition in the raw meal for the production of Portland cement clinker, *J. Hazard. Mater.* 116 (1–2) (2004) 103–110.
- [34] T. Hertel, A. Van den Bulck, S. Onsei, P.P. Sivakumar, Y. Pontikes, Boosting the use of bauxite residue (red mud) in cement - production of an Fe-rich calciumsulfoaluminate-ferrite clinker and characterisation of the hydration, *Cem. Concr. Res.* 145 (2021), 106463.
- [35] S. Singh, M.U. Aswath, R.V. Ranganath, Performance assessment of bricks and prisms: red mud based geopolymer composite, *J. Build. Eng.* 32 (2020), 101462.
- [36] A. Kumar, S. Kumar, Development of paving blocks from synergistic use of red mud and fly ash using geopolymrization, *Constr. Build. Mater.* 38 (2013) 865–871.
- [37] F. Arroyo, Y. Luna-Galiano, C. Leiva, L. Vilches, C. Fernández-Pereira, Environmental risks and mechanical evaluation of recycling red mud in bricks, *Environ. Res.* 186 (2020), 109537.
- [38] M.M. Ahmed, K. El-Naggar, D. Tarek, A. Ragab, H. Sameh, A.M. Zeyad, B.A. Tayeh, I.M. Maafa, A. Yousef, Fabrication of thermal insulation geopolymer bricks using ferrosilicon slag and alumina waste, *Case Stud. Constr. Mater.* 15 (2021), e00737.
- [39] S.Y. Kim, Y. Jun, D. Jeon, J.E. Oh, Synthesis of structural binder for red brick production based on red mud and fly ash activated using Ca(OH)₂ and Na₂CO₃, *Constr. Build. Mater.* 147 (2017) 101–116.
- [40] L. Senff, R. Modolo, A.S. Silva, V. Ferreira, D. Hotza, J. Labrincha, Influence of red mud addition on rheological behavior and hardened properties of mortars, *Constr. Build. Mater.* 65 (2014) 84–91.
- [41] A. Karimpour, H. Jahangir, D. Rezazadeh Eidgahee, A thorough study on the effect of red mud, granite, limestone and marble slurry powder on the strengths of steel fibres-reinforced self-consolidating concrete: experimental and numerical prediction, *J. Build. Eng.* 44 (2021), 103398.
- [42] M. Singh, S. Upadhyay, P. Prasad, Preparation of special cements from red mud, *Waste Manag.* 16 (8) (1996) 665–670.
- [43] C.J. Molineux, D.J. Newport, B. Ayati, C. Wang, S.P. Connop, J.E. Green, Bauxite residue (red mud) as a pulverised fuel ash substitute in the manufacture of lightweight aggregate, *J. Clean. Prod.* 112 (2016) 401–408.
- [44] Y. Sun, J.-s Li, Z. Chen, Q. Xue, Q. Sun, Y. Zhou, X. Chen, L. Liu, C.S. Poon, Production of lightweight aggregate ceramsite from red mud and municipal solid waste incineration bottom ash: mechanism and optimization, *Constr. Build. Mater.* 287 (2021), 122993.
- [45] C. Song, H. Zhang, Y. Dong, L. Pei, H. Liu, J. Jiang, H. Xu, Investigation on the fabrication of lightweight aggregate with acid-leaching tailings of vanadium-bearing stone coal minerals and red mud, *Chin. J. Chem. Eng.* 32 (2021) 353–359.
- [46] B.A. Tayeh, A.M. Zeyad, I.S. Agwa, M. Amin, Effect of elevated temperatures on mechanical properties of lightweight geopolymer concrete, *Case Stud. Constr. Mater.* 15 (2021), e00673.
- [47] A. Agrawal, K. Sahu, B. Pandey, Solid waste management in non-ferrous industries in India, *Resour. Conserv. Recycl.* 42 (2) (2004) 99–120.
- [48] A.M. Zeyad, H.M. Magbool, B.A. Tayeh, A.R.G. de Azevedo, A. Abutaleb, Q. Hussain, Production of geopolymer concrete by utilizing volcanic pumice dust, *Case Stud. Constr. Mater.* 16 (2022), e00802.
- [49] W. Wang, W. Chen, H. Liu, C. Han, Recycling of waste red mud for production of ceramic floor tile with high strength and lightweight, *J. Alloy. Compd.* 748 (2018) 876–881.
- [50] H. Yang, C. Chen, L. Pan, H. Lu, H. Sun, X. Hu, Preparation of double-layer glass-ceramic/ceramic tile from bauxite tailings and red mud, *J. Eur. Ceram. Soc.* 29 (10) (2009) 1887–1894.
- [51] X. Xu, J. Song, Y. Li, J. Wu, X. Liu, C. Zhang, The microstructure and properties of ceramic tiles from solid wastes of Bayer red muds, *Constr. Build. Mater.* 212 (2019) 266–274.
- [52] S. Vigneshwaran, M. Uthayakumar, V. Arumugaprabu, Development and sustainability of industrial waste-based red mud hybrid composites, *J. Clean. Prod.* 230 (2019) 862–868.
- [53] W. Zhou, X. Shi, X. Lu, C. Qi, B. Luan, F. Liu, The mechanical and microstructural properties of refuse mudstone-GGBS-red mud based geopolymer composites made with sand, *Constr. Build. Mater.* 253 (2020), 119193.
- [54] S. Vigneshwaran, M. Uthayakumar, V. Arumugaprabu, Potential use of industrial waste-red mud in developing hybrid composites: a waste management approach, *J. Clean. Prod.* 276 (2020), 124278.
- [55] S.M.A. Qaidi, Behavior of Concrete Made of Recycled PET Waste and Confined with CFRP Fabrics, College of Engineering, University of Duhok, 2021.
- [56] S.M.A. Qaidi, Y.S.S. Al-Kamaki, State-of-the-Art review: concrete made of recycled waste PET as fine aggregate, *J. Duhok Univ.* 23 (2) (2021) 412–429.
- [57] S.-w Bi, Techniques of Alumina Production, Chemical Industry Press, Beijing, 2006 (in Chinese).
- [58] A. MEC (Minerals Education Coalition), Minerals education coalition, 2013.
- [59] T.C. Santini, Chemical and mineralogical aspects of soil formation in bauxite residue, University of Western Australia, 2012.
- [60] F. Meyer, Availability of bauxite reserves, *Nat. Resour. Res.* 13 (3) (2004) 161–172.
- [61] Y. Zhong-yu, Alumina Production Technology, Metallurgical Industry Press, Beijing, 1993.
- [62] G. Power, M. Gräfe, C. Klauber, Bauxite residue issues: I. Current management, disposal and storage practices, *Hydrometallurgy* 108 (1) (2011) 33–45.
- [63] Z. Yu, Y. Chen, Y. Niu, Y. Tang, P. Wan, Z. Lv, X.J. Yang, Efficient and sustainable production of alumina by electrolysis of sodium carbonate, *Angew. Chem.* 123 (49) (2011) 11923–11927.
- [64] S. Panda, R.B. Costa, S.S. Shah, S. Mishra, D. Bevilacqua, A. Akcil, Biotechnological trends and market impact on the recovery of rare earth elements from bauxite residue (red mud)-a review, *Resour. Conserv. Recycl.* 171 (2021), 105645.
- [65] I.A. Institute, Alumina Production, 2022.
- [66] E. Mukiza, L. Zhang, X. Liu, N. Zhang, Utilization of red mud in road base and subgrade materials: a review, *Resour. Conserv. Recycl.* 141 (2019) 187–199.
- [67] H. Sutar, S.C. Mishra, S.K. Sahoo, H.S. Maharana, Progress of red mud utilization: an overview, 2014.
- [68] M. Lima, L. Thives, V. Haritonovs, K. Bajars, Red mud application in construction industry: review of benefits and possibilities. IOP Conference Series: Materials Science and Engineering, IOP Publishing, 2017.
- [69] H. Vijaya, T. Samuel, P. Wesly, Assessment of red mud as a construction material a review, *Indian J. Sci. Res.* 17 (2) (2018) 473–478.
- [70] T. Hertel, A. Van den Bulck, B. Blanpain, Y. Pontikes, Correlating the amorphous phase structure of vitrified bauxite residue (red mud) to the initial reactivity in binder systems, *Cem. Concr. Compos.* (2022), 104410.
- [71] N.C. Gomes Silveira, M.L. Figueiredo Martins, A.Cd.S. Bezerra, F. Gabriel da Silva Araújo, Ecological geopolymer produced with a ternary system of red mud, glass waste, and Portland cement, *Clean. Eng. Technol.* 6 (2022), 100379.
- [72] Y. Liu, R. Naidu, H. Ming, Red mud as an amendment for pollutants in solid and liquid phases, *Geoderma* 163 (1–2) (2011) 1–12.
- [73] R.R. Raja, E. Pillaib, A. Santhakumarc, Effective utilization of red mud bauxite waste as a re-placement of cement in concrete for environmental conservation, *Ecol. Environ. Conserv.* 19 (1) (2013) 247–255.
- [74] M. Khairul, J. Zanganeh, B. Moghtaderi, The composition, recycling and utilisation of Bayer red mud, *Resour. Conserv. Recycl.* 141 (2019) 483–498.
- [75] R. Paramguru, P. Rath, V. Misra, Trends in red mud utilization-a review, *Miner. Process. Extr. Metall. Rev.* 26 (1) (2004) 1–29.
- [76] S. Rai, K. Wasewar, J. Mukhopadhyay, C.K. Yoo, H. Uslu, Neutralization and utilization of red mud for its better waste management, *World* 6 (2012) 5410.
- [77] D.-r Zhang, H.-r Chen, Z.-y Nie, J.-l Xia, E.-p Li, X.-l Fan, L. Zheng, Extraction of Al and rare earths (Ce, Gd, Sc, Y) from red mud by aerobic and anaerobic bi-stage bioleaching, *Chem. Eng. J.* 401 (2020), 125914.
- [78] K. Yoon, D.-W. Cho, Y.F. Tsang, D.C. Tsang, E.E. Kwon, H. Song, Synthesis of functionalised biochar using red mud, lignin, and carbon dioxide as raw materials, *Chem. Eng. J.* 361 (2019) 1597–1604.
- [79] D.-r Zhang, H.-r Chen, J.-l Xia, Z.-y Nie, R.-y Zhang, A. Schippers, W.-s Shu, L.-x Qian, Red mud regulates arsenic fate at acidic pH via regulating arsenopyrite bio-oxidation and S, Fe, Al, Si speciation transformation, *Water Res.* 203 (2021), 117539.
- [80] S. Pascucci, C. Belviso, R.M. Cavalli, A. Palombo, S. Pignatti, F. Santini, Using imaging spectroscopy to map red mud dust waste: the Podgorica Aluminum Complex case study, *Remote Sens. Environ.* 123 (2012) 139–154.

- [81] S. Chauhan, A. Ganguly, Standardizing rehabilitation protocol using vegetation cover for bauxite waste (red mud) in eastern India, *Ecol. Eng.* 37 (3) (2011) 504–510.
- [82] S. Agrawal, N. Dhawan, Evaluation of red mud as a polymetallic source – a review, *Miner. Eng.* 171 (2021), 107084.
- [83] M. Gautam, B. Pandey, M. Agrawal, Identification of indicator species at abandoned red mud dumps in comparison to residential and forest sites, accredited to soil properties, *Ecol. Indic.* 88 (2018) 88–102.
- [84] M. Gautam, M. Agrawal, Identification of metal tolerant plant species for sustainable phytomanagement of abandoned red mud dumps, *Appl. Geochem.* 104 (2019) 83–92.
- [85] S. Xue, W. Ke, F. Zhu, Y. Ye, Z. Liu, J. Fan, W. Hartley, Effect of phosphogypsum and poultry manure on aggregate-associated alkaline characteristics in bauxite residue, *J. Environ. Manag.* 256 (2020), 109981.
- [86] K. Zhou, C. Teng, X. Zhang, C. Peng, W. Chen, Enhanced selective leaching of scandium from red mud, *Hydrometallurgy* 182 (2018) 57–63.
- [87] C. Klauber, N. Harwood, R. Hockridge, C. Middleton, Proposed mechanism for the formation of dust horizons on bauxite residue disposal areas. Essential Readings in Light Metals, Springer, 2016, pp. 951–956.
- [88] X. Kong, Y. Guo, S. Xue, W. Hartley, C. Wu, Y. Ye, Q. Cheng, Natural evolution of alkaline characteristics in bauxite residue, *J. Clean. Prod.* 143 (2017) 224–230.
- [89] C. Klauber, N. Harwood, R. Hockridge, C. Middleton, Proposed mechanism for the formation of dust horizons on bauxite residue disposal areas, 2008.
- [90] M. Ge, H. Wang, A. Schissler, R. Ramani, Measuring pillar width in trona mines using a body wave based in-seam seismic technique, *Int. J. Rock Mech. Min. Sci.* 53 (2012) 10–17.
- [91] J. Huang, L. Lin, Y. Yu, M. Lan, J. Zhang, D. Gao, X. Wang, J. Yang, Technical and Product Evaluation of Industrial Solid Waste, China Standard Press, Beijing, 2014.
- [92] X. Qi, H. Wang, C. Huang, L. Zhang, J. Zhang, B. Xu, F. Li, J.T.A. Junior, Analysis of bauxite residue components responsible for copper removal and related reaction products, *Chemosphere* 207 (2018) 209–217.
- [93] H.I. Gomes, W.M. Mayes, M. Rogerson, D.I. Stewart, I.T. Burke, Alkaline residues and the environment: a review of impacts, management practices and opportunities, *J. Clean. Prod.* 112 (2016) 3571–3582.
- [94] S.P. Varnavas, P.P. Achilleopoulos, Factors controlling the vertical and spatial transport of metal-rich particulate matter in seawater at the outfall of bauxitic red mud toxic waste, *Sci. Total Environ.* 175 (3) (1995) 199–205.
- [95] J.P. Olszewska, K.V. Heal, I.J. Winfield, L.J. Eades, B.M. Spears, Assessing the role of bed sediments in the persistence of red mud pollution in a shallow lake (Kinghorn Loch, UK), *Water Res.* 123 (2017) 569–577.
- [96] W. Mayes, I. Burke, H. Gomes, Á. Antón, M. Molnár, V. Feigl, É. Ujaczki, Advances in understanding environmental risks of red mud after the Ajka spill, Hungary, *J. Sustain. Metall.* 2 (4) (2016) 332–343.
- [97] W.M. Mayes, A.P. Jarvis, I.T. Burke, M. Walton, V. Feigl, O. Klebercz, K. Gruiz, Dispersal and attenuation of trace contaminants downstream of the Ajka bauxite residue (red mud) depository failure, Hungary, *Environ. Sci. Technol.* 45 (12) (2011) 5147–5155.
- [98] B. Wang, J. Ma, D. Wang, Z. Gong, Q. Shi, C. Gao, C. Lu, J. Crittenden, Acid-pretreated red mud for selective catalytic reduction of NO_x with NH₃: insights into inhibition mechanism of binders, *Catal. Today* 376 (2021) 247–254.
- [99] S.F. Kurtoglu, S. Soyer-Uzun, A. Uzun, Utilizing red mud modified by simple treatments as a support to disperse ruthenium provides a high and stable performance for CO_x-free hydrogen production from ammonia, *Catal. Today* 357 (2020) 425–435.
- [100] C. Gao, G. Yang, D. Wang, Z. Gong, X. Zhang, B. Wang, Y. Peng, J. Li, C. Lu, J. Crittenden, Modified red mud catalyst for the selective catalytic reduction of nitrogen oxides: impact mechanism of cerium precursors on surface physicochemical properties, *Chemosphere* 257 (2020), 127215.
- [101] T. Yuzhakova, Á. Rédey, Z. Kovács, A. Utasi, I. Ráduly, L. Dióssy, L. Ráduly, J. Fazakas, Red mud waste storage problems, solution and utilization alternatives, *Glob. J. Adv. Pure Appl. Sci.* 1 (2013).
- [102] G. Xu, X. Ding, M. Kuruppu, W. Zhou, W. Biswas, Research and application of non-traditional chemical stabilizers on bauxite residue (red sand) dust control, a review, *Sci. Total Environ.* 616 (2018) 1552–1565.
- [103] W. Liu, X. Chen, W. Li, Y. Yu, K. Yan, Environmental assessment, management and utilization of red mud in China, *J. Clean. Prod.* 84 (2014) 606–610.
- [104] S. Kumar, R. Kumar, A. Bandopadhyay, Innovative methodologies for the utilisation of wastes from metallurgical and allied industries, *Resour. Conserv. Recycl.* 48 (4) (2006) 301–314.
- [105] L. Pérez-Villarejo, F. Corpas-Iglesias, S. Martínez-Martínez, R. Artiaga, J. Pascual-Cosp, Manufacturing new ceramic materials from clay and red mud derived from the aluminium industry, *Constr. Build. Mater.* 35 (2012) 656–665.
- [106] P.J. Joyce, T. Hertel, A. Goronovski, A.H. Tkaczyk, Y. Pontikes, A. Björklund, Identifying hotspots of environmental impact in the development of novel inorganic polymer paving blocks from bauxite residue, *Resour. Conserv. Recycl.* 138 (2018) 87–98.
- [107] Q. Hong, P. Wang, Z. Chen, Z. Huang, L. Shen, T. Song, Evaluation of red mud as oxygen carrier for chemical looping combustion of methane and biomass in fluidized bed, *Fuel Process. Technol.* 222 (2021), 106964.
- [108] A. Anagnostopoulos, M.E. Navarro, M. Stefanidou, P. Seferlis, G. Gaidajis, Y. Ding, Effect of carbon on the performance of red mud-molten salt composites for thermal management and waste heat recovery applications, *J. Energy Storage* 44 (2021), 103363.
- [109] A. Anagnostopoulos, M.E. Navarro, M. Stefanidou, Y. Ding, G. Gaidajis, Red mud-molten salt composites for medium-high temperature thermal energy storage and waste heat recovery applications, *J. Hazard. Mater.* 413 (2021), 125407.
- [110] S. Wang, H. Jin, Y. Deng, Y. Xiao, Comprehensive utilization status of red mud in China: a critical review, *J. Clean. Prod.* 289 (2021), 125136.
- [111] I. Panda, S. Jain, S.K. Das, R. Jayabalan, Characterization of red mud as a structural fill and embankment material using bioremediation, *Int. Biodeterior. Biodegrad.* 119 (2017) 368–376.
- [112] L. Wang, N. Sun, H. Tang, W. Sun, A review on comprehensive utilization of red mud and prospect analysis, *Minerals* 9 (6) (2019) 362.
- [113] X. Liu, P. Gao, S. Yuan, Y. Lv, Y. Han, Clean utilization of high-iron red mud by suspension magnetization roasting, *Miner. Eng.* 157 (2020), 106553.
- [114] S. Samal, A.K. Ray, A. Bandopadhyay, Characterization and microstructure observation of sintered red mud-fly ash mixtures at various elevated temperature, *J. Clean. Prod.* 101 (2015) 368–376.
- [115] R. Milaćić, T. Zuliani, J. Šćančar, Environmental impact of toxic elements in red mud studied by fractionation and speciation procedures, *Sci. Total Environ.* 426 (2012) 359–365.
- [116] W. Wu, Z. Chen, Y. Huang, J. Li, D. Chen, N. Chen, M. Su, Red mud for the efficient adsorption of U(VI) from aqueous solution: influence of calcination on performance and mechanism, *J. Hazard. Mater.* 409 (2021), 124925.
- [117] A. Kumar, T.J. Saravanan, K. Bisht, K.I.S.A. Kabeer, A review on the utilization of red mud for the production of geopolymers and alkali activated concrete, *Constr. Build. Mater.* 302 (2021), 124170.
- [118] T. Kovács, M. Horváth, A. Csordás, G. Bátor, E. Tóth-Bodrogi, Tobacco plant as possible biomonitoring tool of red mud dust fallout and increased natural radioactivity, *Heliyon* 6 (3) (2020), e03455.
- [119] Z. Chen, W. Wu, N. Chen, D. Chen, M. Su, Uranium stabilization in red mud by sintering: mechanism and leachability, *Ceram. Int.* (2021).
- [120] G.-z Lu, T.-a Zhang, L.-n Ma, Y.-x Wang, W.-g Zhang, Z.-m Zhang, L. Wang, Utilization of Bayer red mud by a calcification–carbonation method using calcium aluminate hydrate as a calcium source, *Hydrometallurgy* 188 (2019) 248–255.
- [121] X. Liu, Y. Han, F. He, P. Gao, S. Yuan, Characteristic, hazard and iron recovery technology of red mud—a critical review, *J. Hazard. Mater.* 420 (2021), 126542.
- [122] G. Power, M. Gräfe, C. Klauber, Bauxite residue issues: I. Current management, disposal and storage practices, *Hydrometallurgy* 108 (1–2) (2011) 33–45.
- [123] S. Wang, Y. Boyjoo, A. Choueib, Z. Zhu, Removal of dyes from aqueous solution using fly ash and red mud, *Water Res.* 39 (1) (2005) 129–138.
- [124] K. Snars, R. Gilkes, Evaluation of bauxite residues (red muds) of different origins for environmental applications, *Appl. Clay Sci.* 46 (1) (2009) 13–20.
- [125] R. Pingping, Analysis on basic characteristics of BAYER • S dry red mud and the operation feature of the yard, *工程地质学报* 18 (3) (2010) 340–344.
- [126] J. Zhang, S. Liu, Z. Yao, S. Wu, H. Jiang, M. Liang, Y. Qiao, Environmental aspects and pavement properties of red mud waste as the replacement of mineral filler in asphalt mixture, *Constr. Build. Mater.* 180 (2018) 605–613.

- [127] K. Komnitsas, G. Bartzas, I. Paspaliaris, Efficiency of limestone and red mud barriers: laboratory column studies, *Miner. Eng.* 17 (2) (2004) 183–194.
- [128] V.K. Gupta, M. Gupta, S. Sharma, Process development for the removal of lead and chromium from aqueous solutions using red mud—an aluminium industry waste, *Water Res.* 35 (5) (2001) 1125–1134.
- [129] S. Agrawal, V. Rayapudi, N. Dhawan, Extraction of iron values from red mud, *Mater. Today Proc.* 5 (9) (2018) 17064–17072.
- [130] S. Alam, B.K. Das, S.K. Das, Dispersion and sedimentation characteristics of red mud, *J. Hazard. Toxic Radioact. Waste* 22 (4) (2018), 04018025.
- [131] S. Suprapto, Z. Istiqomah, E. Santoso, A.A. Dawam, D. Prasetyoko, Alumina extraction from red mud by magnetic separation, *Indones. J. Chem.* 18 (2) (2018) 331–336.
- [132] V.M. Sglavo, R. Campostrini, S. Maurina, G. Carturan, M. Monagheddu, G. Budroni, G. Cocco, Bauxite 'red mud' in the ceramic industry. Part 1: thermal behaviour, *J. Eur. Ceram. Soc.* 20 (3) (2000) 235–244.
- [133] N. Justiz-Smith, V.E. Buchanan, G. Oliver, The potential application of red mud in the production of castings, *Mater. Sci. Eng. A* 420 (1–2) (2006) 250–253.
- [134] D. Zinoveev, P. Grudinsky, E. Zhiltsova, D. Grigoreva, A. Volkov, V. Dyubanov, A. Petelin, Research on high-pressure hydrochloric acid leaching of scandium, aluminum and other valuable components from the non-magnetic tailings obtained from red mud after iron removal, *Metals* 11 (3) (2021) 469.
- [135] A. Collazo, D. Fernández, M. Izquierdo, X. Nóvoa, C. Pérez, Evaluation of red mud as surface treatment for carbon steel prior painting, *Prog. Org. Coat.* 52 (4) (2005) 351–358.
- [136] H.S. Altundoğan, S. Altundoğan, F. Tümen, M. Bildik, Arsenic adsorption from aqueous solutions by activated red mud, *Waste Manag.* 22 (3) (2002) 357–363.
- [137] S. Srikanth, A.K. Ray, A. Bandopadhyay, B. Ravikumar, A. Jha, Phase constitution during sintering of red mud and red mud-fly ash mixtures, *J. Am. Ceram. Soc.* 88 (9) (2005) 2396–2401.
- [138] J. He, J. Zhang, Y. Yu, G. Zhang, The strength and microstructure of two geopolymers derived from metakaolin and red mud-fly ash admixture: a comparative study, *Constr. Build. Mater.* 30 (2012) 80–91.
- [139] S. Agrawal, N. Dhawan, Investigation of mechanical and thermal activation on metal extraction from red mud, *Sustain. Mater. Technol.* 27 (2021), e00246.
- [140] S.-P. Kang, S.-J. Kwon, Effects of red mud and alkali-activated slag cement on efflorescence in cement mortar, *Constr. Build. Mater.* 133 (2017) 459–467.
- [141] HINDALCO, Hindalco to supply 1.2 mn MT of red mud to UltraTech: two flagship Aditya Birla Group companies join hands to promote a circular economy, 2020.
- [142] Y. Liu, R. Naidu, Hidden values in bauxite residue (red mud): recovery of metals, *Waste Manag.* 34 (12) (2014) 2662–2673.
- [143] B. Das, K. Mohanty, A review on advances in sustainable energy production through various catalytic processes by using catalysts derived from waste red mud, *Renew. Energy* 143 (2019) 1791–1811.
- [144] A. Davidovits, Geopolymers: inorganic polymeric new materials, *J. Therm. Anal.* 37 (1991) 1633–1656.
- [145] H.U. Ahmed, A.A. Mohammed, S. Rafiq, A.S. Mohammed, A. Mosavi, N.H. Sor, S. Qaidi, Compressive strength of sustainable geopolymer concrete composites: a state-of-the-art review, *Sustainability* 13 (24) (2021) 13502.
- [146] P. Duxson, A. Fernández-Jiménez, J.L. Provis, G.C. Lukey, A. Palomo, J.S. van Deventer, Geopolymer technology: the current state of the art, *J. Mater. Sci.* 42 (9) (2007) 2917–2933.
- [147] W. Mozgawa, J. Deja, Spectroscopic studies of alkaline activated slag geopolymers, *J. Mol. Struct.* 924–926 (2009) 434–441.
- [148] H. Yan, X. Zhu, F. Dai, Y. He, X. Jing, P. Song, R. Wang, Porous geopolymer based eco-friendly multifunctional slow-release fertilizers for promoting plant growth, *Colloids Surf. A Physicochem. Eng. Asp.* 631 (2021), 127646.
- [149] E.E. Sánchez Díaz, V.A. Escobar Barrios, Development and use of geopolymers for energy conversion: an overview, *Constr. Build. Mater.* 315 (2022), 125774.
- [150] Y. Qin, X. Chen, B. Li, Y. Guo, Z. Niu, T. Xia, W. Meng, M. Zhou, Study on the mechanical properties and microstructure of chitosan reinforced metakaolin-based geopolymer, *Constr. Build. Mater.* 271 (2021), 121522.
- [151] L.O. Afolabi, Z.M. Ariff, P.S.M. Megat-Yusoff, H.H. Al-Kayiem, A.I. Arogundade, O.T. Afolabi-Owolabi, Red-mud geopolymer composite encapsulated phase change material for thermal comfort in built-sector, *Sol. Energy* 181 (2019) 464–474.
- [152] H.U. Ahmed, A.A. Mohammed, S. Rafiq, A.S. Mohammed, A. Mosavi, N.H. Sor, S.M.A. Qaidi, Compressive strength of sustainable geopolymer concrete composites: a state-of-the-art review, *Sustainability* 13 (24) (2021) 13502.
- [153] S.M.A. Qaidi, Y.Z. Dinkha, J.H. Haido, M.H. Ali, B.A. Tayeh, Engineering properties of sustainable green concrete incorporating eco-friendly aggregate of crumb rubber: a review, *J. Clean. Prod.* (2021), 129251.
- [154] S.M.A. Qaidi, B.A. Tayeh, A.M. Zeyad, A.R.G. de Azevedo, H.U. Ahmed, W. Emad, Recycling of mine tailings for the geopolymers production: a systematic review, *Case Stud. Constr. Mater.* (2022).
- [155] O. Zaid, F.M. Mukhtar, R. Martínez-García, M.G. El Sherbiny, A.M. Mohamed, Characteristics of high-performance steel fiber reinforced recycled aggregate concrete utilizing mineral filler, *Case Stud. Constr. Mater.* (2022), e00939.
- [156] P. Zhang, K. Wang, Q. Li, J. Wang, Y. Ling, Fabrication and engineering properties of concretes based on geopolymers/alkali-activated binders-a review, *J. Clean. Prod.* 258 (2020), 120896.
- [157] P.N. Lemounga, K.-t Wang, Q. Tang, X.-m Cui, Study on the development of inorganic polymers from red mud and slag system: application in mortar and lightweight materials, *Constr. Build. Mater.* 156 (2017) 486–495.
- [158] A. Bayat, A. Hassani, A. Yousefi, Effects of red mud on the properties of fresh and hardened alkali-activated slag paste and mortar, *Constr. Build. Mater.* 167 (2018) 775–790.
- [159] J. Zhang, S. Li, Z. Li, C. Liu, Y. Gao, Feasibility study of red mud for geopolymer preparation: effect of particle size fraction, *J. Mater. Cycles Waste Manag.* 22 (5) (2020) 1328–1338.
- [160] Z. Pan, D. Li, J. Yu, N. Yang, Properties and microstructure of the hardened alkali-activated red mud–slag cementitious material, *Cem. Concr. Res.* 33 (9) (2003) 1437–1441.
- [161] K. Hyeok-Jung, S.-P. Kang, G.-C. Choe, Effect of red mud content on strength and efflorescence in pavement using alkali-activated slag cement, *Int. J. Concr. Struct. Mater.* 12 (1) (2018) 1–9.
- [162] S. Singh, M. Aswath, R. Ranganath, Performance assessment of bricks and prisms: red mud based geopolymer composite, *J. Build. Eng.* 32 (2020), 101462.
- [163] C. Lin, W. Dai, Z. Li, F. Sha, Performance and microstructure of alkali-activated red mud-based grouting materials under class F fly ash amendment, *Indian Geotech. J.* 50 (6) (2020) 1048–1056.
- [164] P. Mpofu, J. Addai-Mensah, J. Ralston, Investigation of the effect of polymer structure type on flocculation, rheology and dewatering behaviour of kaolinite dispersions, *Int. J. Miner. Process.* 71 (1–4) (2003) 247–268.
- [165] N. Ye, J. Yang, X. Ke, J. Zhu, Y. Li, C. Xiang, H. Wang, L. Li, B. Xiao, Synthesis and characterization of geopolymer from Bayer red mud with thermal pretreatment, *J. Am. Ceram. Soc.* 97 (5) (2014) 1652–1660.
- [166] X. Cheng, D. Long, C. Zhang, X. Gao, Y. Yu, K. Mei, C. Zhang, X. Guo, Z. Chen, Utilization of red mud, slag and waste drilling fluid for the synthesis of slag-red mud cementitious material, *J. Clean. Prod.* 238 (2019), 117902.
- [167] S. Ahmed, T. Meng, M. Taha, Utilization of red mud for producing a high strength binder by composition optimization and nano strengthening, *Nanotechnol. Rev.* 9 (1) (2020) 396–409.
- [168] Z. Li, J. Zhang, S. Li, Y. Gao, C. Liu, Y. Qi, Effect of different gypsums on the workability and mechanical properties of red mud–slag based grouting materials, *J. Clean. Prod.* 245 (2020), 118759.
- [169] X. Chen, Y. Guo, S. Ding, H. Zhang, F. Xia, J. Wang, M. Zhou, Utilization of red mud in geopolymer-based pervious concrete with function of adsorption of heavy metal ions, *J. Clean. Prod.* 207 (2019) 789–800.
- [170] A. Bayat, A. Hassani, O. Azami, Thermo-mechanical properties of alkali-activated slag–red mud concrete, *Road Mater. Pavement Des.* 21 (2) (2020) 411–433.
- [171] R. He, N. Dai, Z. Wang, Thermal and mechanical properties of geopolymers exposed to high temperature: a literature review, *Adv. Civ. Eng.* 2020 (2020).
- [172] F. Longo, P. Lassandro, A. Moshiri, T. Phatak, M.A. Aiello, K.J. Krakowiak, Lightweight geopolymer-based mortars for the structural and energy retrofit of buildings, *Energy Build.* 225 (2020), 110352.

- [173] H.T. Nguyen, S.M. Gallardo, F. Bacani, H. Hinode, Q.M. Do, M.A. Promentilla, Evaluating thermal properties of geopolymer produced from red mud, rice husk ash and diatomaceous earth, *ASEAN Eng. J.* 4 (1) (2015) 51–65.
- [174] P. Krivenko, O. Kovalchuk, A. Pasko, T. Croymans, M. Hult, G. Lutter, N. Vandevenne, S. Schreurs, W. Schroevers, Development of alkali activated cements and concrete mixture design with high volumes of red mud, *Constr. Build. Mater.* 151 (2017) 819–826.
- [175] E. Jamieson, B. McLellan, A. Van Riessen, H. Nikraz, Comparison of embodied energies of Ordinary Portland Cement with Bayer-derived geopolymer products, *J. Clean. Prod.* 99 (2015) 112–118.
- [176] E. Jamieson, B. Penna, A. Van Riessen, H. Nikraz, The development of Bayer derived geopolymers as artificial aggregates, *Hydrometallurgy* 170 (2017) 74–81.
- [177] A. Mellado, C. Catalán, N. Bouzon, M. Borrachero, J. Monzo, J. Payá, Carbon footprint of geopolymeric mortar: study of the contribution of the alkaline activating solution and assessment of an alternative route, *RSC Adv.* 4 (45) (2014) 23846–23852.
- [178] A. Peys, H. Rahier, Y. Pontikes, Potassium-rich biomass ashes as activators in metakaolin-based inorganic polymers, *Appl. Clay Sci.* 119 (2016) 401–409.
- [179] I. Ismail, S.A. Bernal, J.L. Provis, R. San Nicolas, S. Hamdan, J.S. van Deventer, Modification of phase evolution in alkali-activated blast furnace slag by the incorporation of fly ash, *Cem. Concr. Compos.* 45 (2014) 125–135.
- [180] C. Klauber, M. Grafe, G. Power, Low grade bauxite issues: II. options for residue utilization, *J. Hydrometall.* 108 (2011) 11–32.
- [181] A. Gorovski, J. Vind, V. Vassiliadou, D. Panias, A. Tkaczyk, Radiological assessment of the Bayer process, *Miner. Eng.* 137 (2019) 250–258.
- [182] C. Nuccetelli, Y. Pontikes, F. Leonardi, R. Trevisi, New perspectives and issues arising from the introduction of (NORM) residues in building materials: a critical assessment on the radiological behaviour, *Constr. Build. Mater.* 82 (2015) 323–331.
- [183] W. Schroevers, Z. Sas, G. Bator, R. Trevisi, C. Nuccetelli, F. Leonardi, S. Schreurs, T. Kovacs, The NORM4Building database, a tool for radiological assessment when using by-products in building materials, *Constr. Build. Mater.* 159 (2018) 755–767.
- [184] Z. Sas, W. Sha, M. Soutsos, R. Doherty, D. Bondar, K. Gijbels, W. Schroevers, Radiological characterisation of alkali-activated construction materials containing red mud, fly ash and ground granulated blast-furnace slag, *Sci. Total Environ.* 659 (2019) 1496–1504.
- [185] T. Hertel, Y. Pontikes, Geopolymers, inorganic polymers, alkali-activated materials and hybrid binders from bauxite residue (red mud)—putting things in perspective, *J. Clean. Prod.* 258 (2020), 120610.
- [186] T. Croymans, W. Schroevers, P. Krivenko, O. Kovalchuk, A. Pasko, M. Hult, G. Marissens, G. Lutter, S. Schreurs, Radiological characterization and evaluation of high volume bauxite residue alkali activated concretes, *J. Environ. Radioact.* 168 (2017) 21–29.
- [187] J. Beretka, P. Matthew, Natural radioactivity of Australian building materials, industrial wastes and by-products, *Health Phys.* 48 (1) (1985) 87–95.
- [188] M. Cooper, P. Clarke, W. Robertson, I. McPharlin, R. Jeffrey, An investigation of radionuclide uptake into food crops grown in soils treated with bauxite mining residues, *J. Radioanal. Nucl. Chem.* 194 (2) (1995) 379–387.
- [189] H. Gu, N. Wang, S. Liu, Radiological restrictions of using red mud as building material additive, *Waste Manag. Res.* 30 (9) (2012) 961–965.
- [190] K. Wang, Levels of radioactivity in the red mud and red mud cement and its send out to local residents, *Environ. Sci.* 13 (1992) 90–93.
- [191] V. Cuccia, Z. Rocha, A.H.d. Oliveira, Radionuclides in Bayer process residues: previous analysis for radiological protection, 2011.
- [192] H. Von Philipsborn, E. Kühnast, Gamma spectrometric characterisation of industrially used African and Australian bauxites and their red mud tailings, *Radiat. Prot. Dosim.* 45 (1–4) (1992) 741–743.
- [193] M. Samouhos, M. Taxiarhou, P.E. Tsakiridis, K. Potiriadis, Greek “red mud” residue: a study of microwave reductive roasting followed by magnetic separation for a metallic iron recovery process, *J. Hazard. Mater.* 254 (2013) 193–205.
- [194] Y. Pontikes, I. Vangelatos, D. Boufounos, D. Fafoutis, G. Angelopoulos, Environmental aspects on the use of Bayer's process bauxite residue in the production of ceramics, *Advances in Science and Technology, Trans Tech Publ.*, 2006, pp. 2176–2181.
- [195] I.B.f.E.S. (IBES), Assessment of environmental risk for use of radioactively contaminated industrial tailings, 2011.
- [196] J. Somlai, V. Jobbagy, J. Kovacs, S. Tarján, T. Kovács, Radiological aspects of the usability of red mud as building material additive, *J. Hazard. Mater.* 150 (3) (2008) 541–545.
- [197] A. Akinci, R. Artir, Characterization of trace elements and radionuclides and their risk assessment in red mud, *Mater. Charact.* 59 (4) (2008) 417–421.
- [198] F. Trotti, C. Zampieri, C. Nuccetelli, S. Risica, Review of Italian NORM industries with specific reference to their environmental impact, in: Proceeding of “EAN NORM Workshop—European ALARA Network for NORM”, 2007, pp. 20–22.
- [199] W.R. Pinnock, Measurements of radioactivity in Jamaican building materials and gamma dose equivalents in a prototype red mud house, *Health Phys.* 61 (5) (1991) 647–651.